The S. pombe CDK5 ortholog Pef1 regulates sexual differentiation through control of the TORC1 pathway and autophagy

Matsuda, Shinya
Kikkawa, Ushio
Uda, Haruka
Nakashima, Akio

(Citation)
Journal of Cell Science,133(17):jcs247817

(Issue Date)
2020-09-09

(Resource Type)
journal article

(Version)
Version of Record

(URL)
https://hdl.handle.net/20.500.14094/90009491

© 2020. Published by The Company of Biologists Ltd | Journal of Cell Science (2020) 133, jcs247817. doi:10.1242/jcs.247817

RESEARCH ARTICLE

The *S. pombe* CDK5 ortholog Pef1 regulates sexual differentiation through control of the TORC1 pathway and autophagy

Shinya Matsuda[1,2,*], Ushio Kikkawa[1,3], Haruka Uda[3] and Akio Nakashima[1,3,*]

ABSTRACT

In *Schizosaccharomyces pombe*, a general strategy for survival in response to environmental changes is sexual differentiation, which is triggered by TORC1 inactivation. However, mechanisms of TORC1 regulation in fission yeast remain poorly understood. In this study, we found that Pef1, which is an ortholog of mammalian CDK5, regulates the initiation of sexual differentiation through positive regulation of TORC1 activity. Conversely, deletion of *pef1* leads to activation of autophagy and subsequent excessive TORC1 reactivation during the early phases of the nitrogen starvation response. This excessive TORC1 reactivation results in the silencing of the Ste11-Mei2 pathway and mating defects. Additionally, we found that *pef1* genetically interacts with *tsc1* and *tsc2* for TORC1 regulation, and physically interacts with three cyclins, Clg1, Pas1 and Psl1. The double deletion of *clg1* and *pas1* promotes activation of autophagy and TORC1 during nitrogen starvation, similar to what is seen in *pef1Δ* cells. Overall, our work suggests that Pef1–Clg1 and Pef1–Pas1 complexes regulate initiation of sexual differentiation through control of the TSC–TORC1 pathway and autophagy.

KEY WORDS: Sexual differentiation, Pef1, CDK5, TORC1, Autophagy, Cyclin

INTRODUCTION

In the fission yeast *Schizosaccharomyces pombe*, sexual differentiation is an essential process in order to transmit genetic information to future generations. This process is accompanied by alterations in both morphology and genetic dynamics, which are required to adapt to environmental changes (Davey, 1998; Egel et al., 1990; Engebrecht, 2003; Merlini et al., 2013). Nitrogen starvation leads to alterations in gene expression that lead to conjugation of haploid cells of the opposite mating types or cause cells to enter the G0 quiescent phase (Mata and Bähler, 2006; Marguerat et al., 2012; Sajiki et al., 2009; Shimanuki et al., 2007). In response to nitrogen starvation, the transcription factor Ste11 is activated and translocates from the cytoplasm to the nucleus, facilitating the expression of genes that encode mating pheromones and pheromone receptors, as well as a positive feedback to further transcribe Ste11 (Anandhakumar et al., 2013; Mata and Bähler, 2006; Qin et al., 2003; Sugimoto et al., 1991). Activated Ste11 also upregulates the expression of the *mei2* gene, which encodes an RNA-binding protein that is a key regulator of meiosis and mediates the progression of successive sexual differentiation programs including meiotic division and sporulation (Qin et al., 2003; Sugimoto et al., 1991). Therefore, upregulation of Ste11 is a key event in the initiation of sexual differentiation in *S. pombe*.

Target of rapamycin complex 1 (TORC1) is a strong suppressor of the initiation of sexual differentiation in nutrient-rich conditions through both the inhibition of the nuclear accumulation of Ste11 and the promotion of the degradation of Mei2 by the ubiquitin-proteasome system (Otsubo et al., 2014, 2017; Valbuena and Moreno, 2010). TORC1, which is a kinase complex, is highly conserved between yeast and humans. Misregulation of TORC1 leads to various disorders, including cancer, type-2 diabetes and neurological disorders (Saxton and Sabatini, 2017).

In *S. pombe*, the TORC1 consists of the catalytic subunit, Tor2 [an ortholog of the mechanistic TOR (mTOR) in mammals], Mip1 (Raptor) and Wat1 (mLst8) (Matsuo et al., 2007; Takahara and Maeda, 2012), and its kinase activity is partially inhibited by the rapamycin–FKBP12 complex (Nakashima et al., 2010, 2012; Takahara and Maeda, 2012). Similar to the regulation of TORC1 in mammals, TORC1 in *S. pombe* localizes on the surface of vacuole (yeast lysosome), and is activated through interactions with Rhb1 (in mammals, Rheb GTPase), an essential activator of TORC1 in response to nitrogen sources (Murai et al., 2009; Urano et al., 2005, 2007; Uritani et al., 2006; Valbuena et al., 2012). The TSC complex, which is comprised of Tsc1 and Tsc2, negatively regulates TORC1, as it acts as a GTPase-activating protein (GAP) for Rhb1 (Chia et al., 2017; Ma et al., 2013; Matsumoto et al., 2002; van Slegtenhorst et al., 2004). Rag GTPases and Ragulator are essential for anchoring TORC1 to the lysosome and vacuole membrane in mammals and budding yeast, respectively. However, a recent study suggested that in fission yeast, the Rag GTPases Gtr1 and Gtr2 and Ragulator components Lam1–Lam4 are dispensable for the vacuolar localization of TORC1 and attenuate TORC1 activity to maintain the normal growth of cells (Chia et al., 2017). In addition to these TORC1 regulatory systems, recent reports suggest that tRNA precursors regulate TORC1 activity in response to nutrients to prevent the initiation of sexual differentiation (Otsubo et al., 2018). Thus, fission yeast is an excellent model organism because various unique TORC1 regulatory mechanisms have been identified. However, there is little information about the role of TORC1 in the regulation of sexual differentiation.

Under nutrient-rich conditions, TORC1 promotes protein synthesis via direct phosphorylation of Thr-415 of the ribosomal protein S6 kinase Psk1 (Nakashima et al., 2012), which is the equivalent of mammalian p70S6K (also known as RPS6KB1) phosphorylation at Thr-389. TORC1 in *S. pombe* also suppresses the initiation of autophagy through phosphorylation of Atg13 (Otsubo et al., 2017, 2018), similar to what is found in budding yeast and mammals. Autophagy acts as a bulk degradation system, but also plays an

[1]Biosignal Research Center, Kobe University, Kobe, 657-8501, Japan. [2]Department of Pharmaceutical Sciences, University of Shizuoka, Shizuoka, 422-8526, Japan. [3]Department of Bioresource Science, Graduate School of Agricultural Science, Kobe University, Kobe, 657-8501, Japan.

*Authors for correspondence (s-matsuda@u-shizuoka-ken.ac.jp; anakashima@person.kobe-u.ac.jp)

S.M., 0000-0002-0169-1347; A.N., 0000-0002-4651-8548

Handling Editor: John Heath
Received 23 April 2020; Accepted 20 July 2020

Journal of Cell Science (2020) 133, jcs247817. doi:10.1242/jcs.247817

important role in driving the sexual differentiation process, as degraded proteins or organelles can be utilized as nutrient sources for promoting sexual differentiation (Mukaiyama et al., 2010). In addition, recycled nutrients reactivate TORC1 to terminate autophagy under starvation conditions (Shin and Huh, 2011; Yu et al., 2010). Thus, expanding knowledge about the regulatory mechanisms of balance between TORC1 activity and autophagy can provide essential insight into the mechanisms of sexual differentiation in fission yeast.

Cyclin-dependent kinases (CDKs) are Ser/Thr kinases that play a central role in cell cycle progression, and their activity is controlled

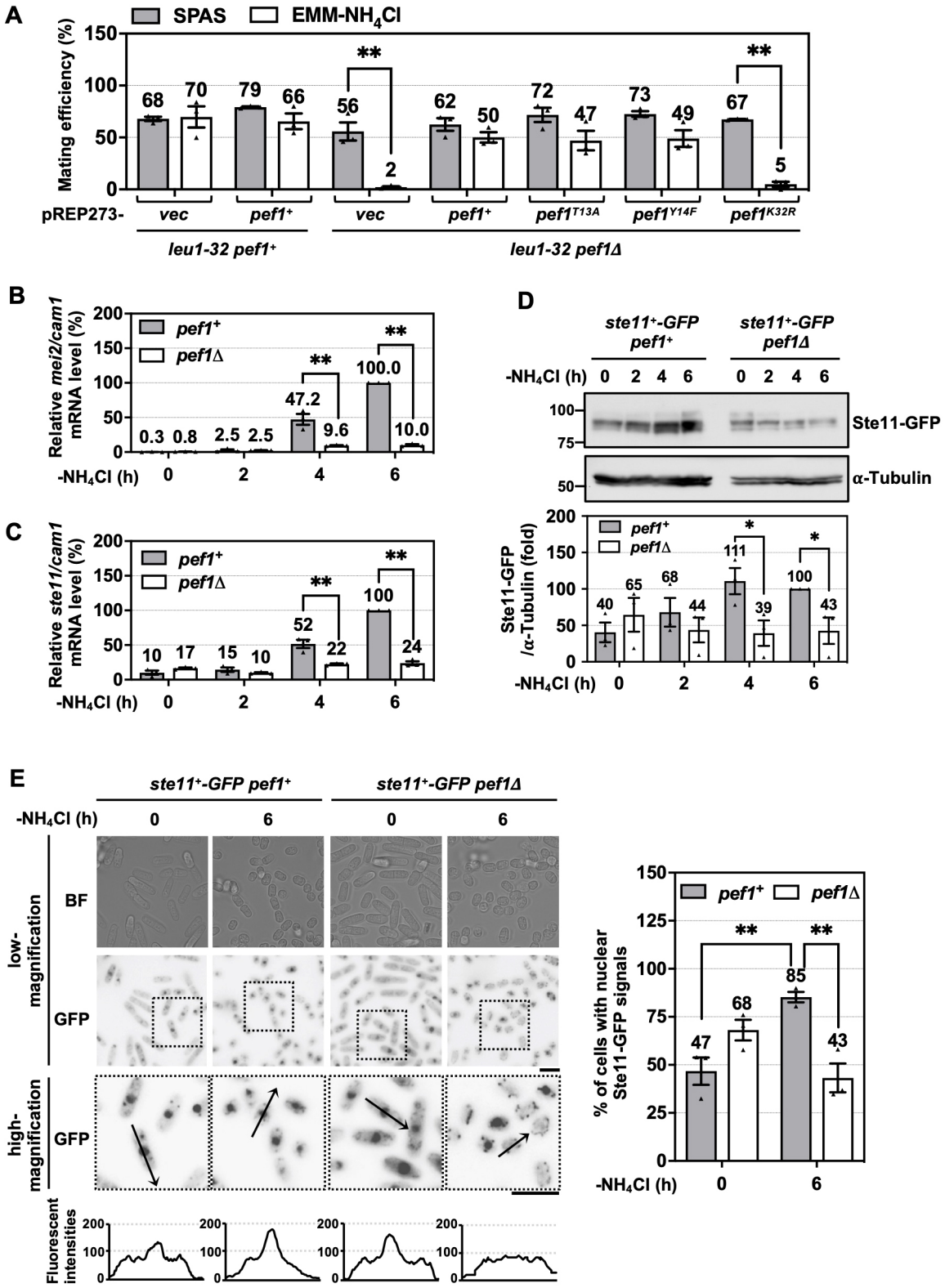

Fig. 1. See next page for legend.

Journal of Cell Science (2020) 133, jcs247817. doi:10.1242/jcs.247817

Fig. 1. The deletion of *pef1* suppresses activation of Ste11 during nitrogen starvation. (A) *leu1-32 pef1*$^{+}$ and *leu1-32 pef1Δ* strains transformed with pREP273 empty vector (vec, MS61 and MS64), *pef1*$^{+}$(MS62 and MS83), *pef1*^{T13A} (MS84), *pef1*^{Y14F} (MS85) or *pef1*^{K32R} (MS86) were cultured on SPAS or EMM-NH_4Cl agar for 2 days at 25°C. The fixed cells were stained with DAPI to measure mating efficiencies. Results are expressed as means±s.e.m. from three independent experiments (at least 100 cells were counted for each genotype and condition). ***P*<0.01 (Student's *t*-tests). (B,C) *pef1*$^{+}$ (L972) and *pef1Δ* (MS9) strains were incubated in EMM-NH_4Cl for the indicated times. Each cDNA was subjected to qPCR analysis. mRNA levels of *cam1* were monitored as a loading control. Normalized mRNA levels of *ste11* or *mei2* at 6 h of nitrogen starvation in *pef1*$^{+}$ cells was taken as 100%. Results are expressed as means±s.e.m. from three independent experiments. ***P*<0.01 (Student's *t*-test). (D,E) *ste11*$^{+}$*-GFP pef1*$^{+}$ (MS145) and *pef1Δ* (MS146) cells were cultured in EMM-NH_4Cl for the indicated times. (D) The cell lysates were subjected to western blot analysis using anti-GFP antibody. α-tubulin was employed as a loading control. Normalized Ste11 expression level at 6 h of nitrogen starvation in *pef1*$^{+}$ cells was taken as 100%. Results are expressed as means±s.e.m. from three independent experiments. **P*<0.05 (Student's *t*-test). (E) These cells were also incubated in EMM or EMM-NH_4Cl. Fluorescence is shown as gray. All images including bright-field (BF) were obtained using a 60× objective lens. Digitally 2–3 times magnified images are shown in the lower panel. Fluorescence detected by line profile imaging along the black arrow were plotted as a Ste11–GFP localization. Having fluorescence in the nucleus were regarded as the nuclear Ste11–GFP signals (graph on right). Results are expressed as means±s.e.m. from three independent experiments (at least 200 cells were counted for each genotype and condition). ***P*<0.01 (one-way ANOVA). Scale bars: 10 µm.

by cyclins, other kinases and phosphatases (Malumbres and Barbacid, 2005). In *S. pombe*, *pombe* pho eighty-five 1 (Pef1) is a member of the CDK5 subfamily, which includes budding yeast PHO85, and mammalian CDK5 and CDK14–CDK18 (Cao et al., 2014). Unlike canonical cell cycle-related CDKs (e.g. CDK1 and CDK2), the CDK5 subfamily members are involved in the regulation of various cellular functions in post-mitotic cells, such as spermatogenesis, cell migration and autophagy (Cao et al., 2014; Dhavan and Tsai, 2001; Matsuda et al., 2017; Mikolcevic et al., 2012; Yang et al., 2010). Although reports suggest that Pef1 controls cell cycle and chronological life span and interacts with three cyclins, Clg1, Pas1 and Psl1 (Chen et al., 2013; Tanaka and Okayama, 2000), the downstream signaling pathway and activation mechanisms of Pef1 remain unclear. To expand the understanding of Pef1 function, we examined the role of *pef1* deletion on cellular function. We found that Pef1 is involved in the regulation of mating efficiency through upregulation of the Ste11-Mei2 pathway. *pef1* deletion reduced TORC1 activity during vegetative growth conditions but promoted autophagy and TORC1 reactivation during nitrogen starvation. Double deletion of *clg1* and *pas1* promoted autophagy and TORC1 reactivation as was seen in *pef1*-deficient cells, indicating that Clg1 and Pas1 are activators of Pef1 during the initiation of sexual differentiation. Our results provide new insight into the Pef1-mediated sexual differentiation machinery.

RESULTS

Pef1 controls mating efficiency through activation of the Ste11-Mei2 pathway

Although kinases closely related to CDK5 (for instance mammalian CDK14–CDK18 or budding yeast PHO85) are involved in the regulation of various signal transduction pathways in post-mitotic cells (Cao et al., 2014; Dhavan and Tsai, 2001; Matsuda et al., 2017; Mikolcevic et al., 2012; Yang et al., 2010), the biological role and signaling pathways regulated by *S. pombe* Pef1 remain unclear. To examine the physiological functions of Pef1, we constructed a *pef1*-deficient strain and introduced LEU2-based pREP273 vectors encoding 3HA-tagged forms of Pef1 mutants into *leu1-32 pef1Δ* cells (Nakashima et al., 2014). Western blot analysis confirmed that endogenous Pef1 was not present in the *pef1Δ* strain and that there were similar levels of expression in Pef1-3HA mutants in *pef1* mutant-introduced *pef1Δ* cells (Fig. S1A).

In order to determine mating efficacy, strains were grown on sporulation agar with supplements (SPAS), which contains small amounts of amino acids for efficient mating and sporulation, or Edinburgh minimal medium (EMM) without NH_4Cl (EMM-NH_4Cl) agar, a nitrogen-free medium. As seen in Fig. 1A, there were no differences in the mating efficiency in control cells between SPAS and EMM-NH_4Cl agar. Interestingly, the mating ability of *pef1Δ* cells was significantly decreased on the EMM-NH_4Cl agar as compared to the mating ability on the SPAS. This low mating efficiency in *pef1Δ* cells was restored by the expression of wild-type Pef1 (Pef1 WT), but not Pef1 K32R, which is a mutant that lacks kinase activity. Pef1 has two predicted phosphorylation sites, Thr-13 and Tyr-14, which correspond to Thr-14 and Tyr-15 of Cdc2 (Birot, 2016). Thus, we assessed the effect of phosphorylation of Pef1 on mating efficiency. The mating efficiency of these mutant (Pef1 T13A and Y14F)-expressing cells was unaltered as compared with Pef1 WT expressing cells on both the SPAS and EMM-NH_4Cl agar. These results suggest that Pef1 is required for mating processes in the absence of nitrogen sources. Thus, we suspected that nitrogen starvation evokes the phenotypes seen upon *pef1* deletion. However, a potential phosphorylation of Pef1 at Thr-13 and Thr-14 does not seem to affect mating efficiency during sexual differentiation.

To determine the cause of low mating efficiency in *pef1Δ* cells, we examined the Ste11-Mei2 pathway, since it is known to play a critical role in switching sexual differentiation from mitosis. Ste11 is the upstream transcription factor of Mei2, and its expression levels are significantly increased upon nitrogen starvation (Anandhakumar et al., 2013; Mata and Bähler, 2006; Qin et al., 2003; Sugimoto et al., 1991). Quantitative (q)PCR analysis showed that the mRNA levels of *ste11* and *mei2* were increased after 4 h of starvation in control cells (*pef1*$^{+}$), whereas the expression of these genes in the *pef1Δ* strain was silenced at all times in starved cells (Fig. 1B,C). Additionally, western blot analysis also revealed that the expression of Ste11 were increased by nitrogen starvation in a time-dependent manner, but this effect was strongly suppressed by *pef1* deletion (Fig. 1D). In addition, the percentage of cells with nuclear accumulation of Ste11–GFP was decreased in *pef1Δ* cells at 6 h after nitrogen starvation as compared with control cells (Fig. 1E). These data indicate that Pef1 regulates the initiation of sexual differentiation by activating the Ste11-Mei2 pathway.

pef1 deletion promotes autophagy

Next, we constructed a *pef1*$^{+}$*-GFP* strain to obtain information about the subcellular localization of Pef1. Before the fluorescence microscopy analysis, the cells were stained with FM4-64 to visualize the vacuole. We observed that Pef1 localized in the cytoplasm and nucleus, and as well as having a punctate expression adjacent to vacuoles (indicated as a white arrowhead) (Fig. 2A; Fig. S1B). These puncta near vacuoles were abolished after treatment with rapamycin (Fig. 2B). In addition, the vacuoles in *pef1Δ* cells were smaller than those of control cells (Fig. 2C; Fig. S1C). The vacuole is an essential organelle for autophagic degradation of unnecessary cellular components; thus, we hypothesized that *pef1* is involved in regulation of autophagy. To examine pre-autophagosomal structure (PAS) formation, we created a *pef1Δ GFP-atg8*$^{+}$ double mutant, as Atg8 is the ortholog to proteins of the mammalian LC3 family, which are required for autophagosome

Journal of Cell Science (2020) 133, jcs247817. doi:10.1242/jcs.247817

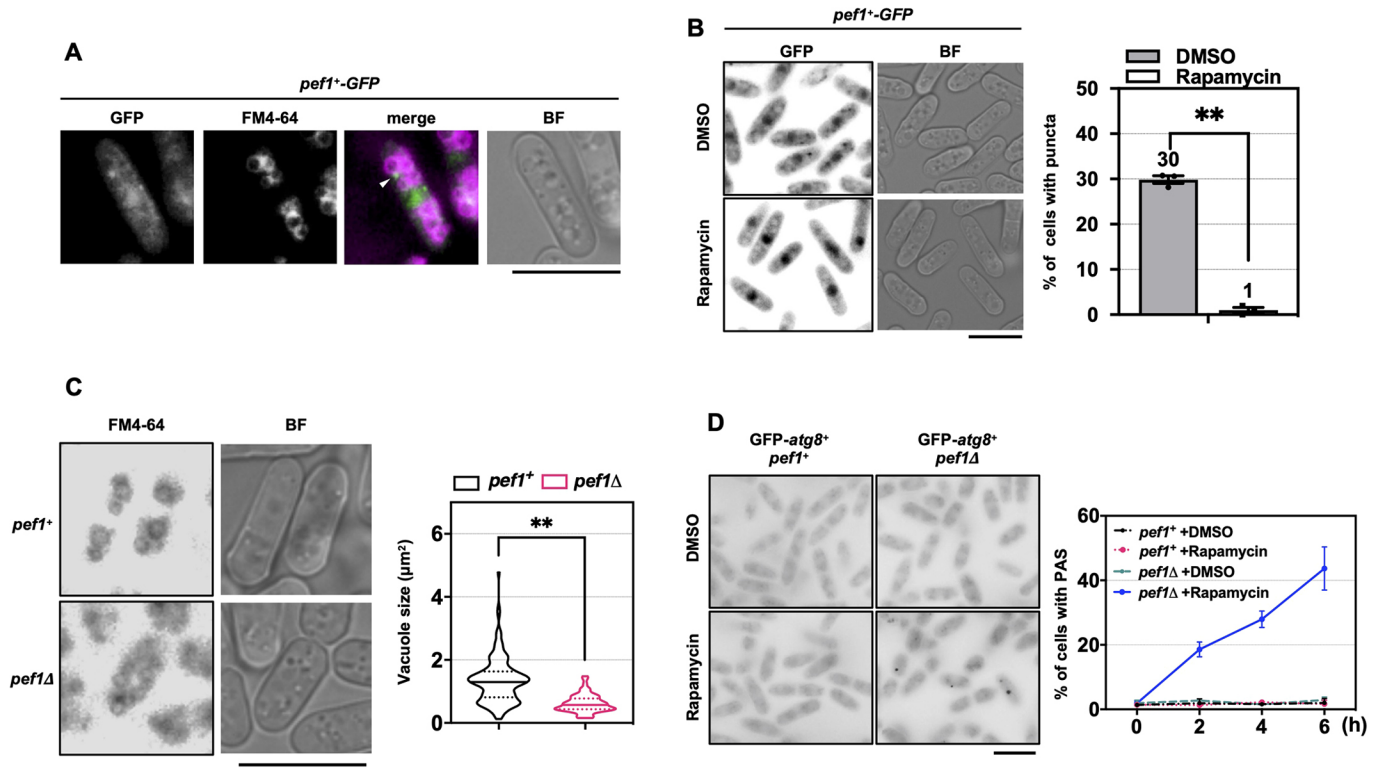

Fig. 2. Pef1 suppresses rapamycin-induced PAS formation. (A) Pef1–GFP-expressing cells (MS51) were stained with FM4-64 and subsequently incubated in EMM. The cells were observed using fluorescence microscopy. Pef1–GFP and FM4-64 are shown as green and magenta, respectively. White arrowhead, punctate expression adjacent to a vacuole. (B) Pef1–GFP-expressing cells (MS51) were incubated in EMM with DMSO or 200 nM rapamycin at 30°C for 6 h. Fluorescence is shown as gray. The percentage of cells with puncta is expressed as means±s.e.m. from three independent experiments (at least 100 cells were counted for each condition). ***P*<0.01 (Student's *t*-test). (C) *pef1*$^+$ (L972) and *pef1Δ* (MS9) strains were stained with FM4-64 and subsequently incubated in EMM. Fluorescence is shown as gray. Vacuole size (μm^2) was measured by use of the BZ-analyzer. Analysis data are displayed as a violin plot. Solid lines represent medians and broken lines represent interquartile ranges; at least 100 vacuoles were measured for each genotype. ***P*<0.01 (Student's *t*-test). (D) *GFP-atg8*$^+$ *pef1*$^+$ (JT268) and *pef1Δ* (MS29) strains were incubated in EMM with DMSO or 200 nM rapamycin for indicated times. The fluorescence of GFP is shown as gray. The percentage of cells with PAS is expressed as means±s.e.m. from three independent experiments (at least 100 cells were counted for each genotype and condition). Scale bars: 10 μm.

maturation (Mukaiyama et al., 2010). Consistent with previous findings, PAS formation was unaffected by rapamycin treatment in control cells (Mukaiyama et al., 2010; Takahara and Maeda, 2012), whereas *pef1* deletion increased PAS signals in response to rapamycin treatment (Fig. 2D). Western blot analysis confirmed that the amounts of truncated GFP, which is the product of autophagically degraded GFP–Atg8, were increased by rapamycin treatment in *pef1Δ* cells; however, there were no differences in autophagic activity in control cells (Fig. 3A). Additionally, the autophagic activity in *pef1Δ* cells during vegetative growth and the early phases of starvation (at 0.5–1 h without NH_4Cl) was slightly higher than that of control cells (Fig. 3B,C). However, the amount of degraded GFP–Atg8 at the late phase of nitrogen starvation was not significantly different between *pef1Δ* cells and in the control cells (Fig. 3B,C), suggesting that *pef1* suppresses autophagy at steady state and the early phase of nitrogen starvation.

To verify that the inactivation of TORC1 is responsible for the increase in autophagic activity in *pef1Δ* cells, we increased Tor2 expression in *pef1Δ* cells by using a pAL-KS-*tor2*$^+$ vector. PAS signals were increased by treatment with rapamycin in *pef1Δ* cells, but these signals were suppressed by expression of Tor2 (Fig. S2A,B). The amount of truncated GFP was also partially decreased by the expression of Tor2 in *pef1Δ* cells (Fig. S2C), indicating that Pef1 might also regulate autophagy by partially suppressing TORC1 activity. Moreover, dephosphorylation and expression of Atg13 appeared to be increased upon *pef1* deletion (Fig. 3A–C). To investigate phosphorylation levels of Atg13, we constructed an Atg13–3HA-expressing strain. As shown in Fig. 3D, Atg13–3HA was detected as sharp bands (labeled 1–3) between 130 kDa and 100 kDa. Although rapamycin stimulation did not detectably lead to a dephosphorylation of Atg13 in *pef1*$^+$ cells, the dephosphorylation of Atg13 was promoted in *pef1Δ* cells as compared to rapamycin-stimulated *pef1*$^+$ cells, indicating that Pef1 suppresses the phosphorylation of Atg13. However, Tor2 expression was unable to restore the expression of Atg13 (Fig. S2C). This result suggests that Pef1 controls the expression of Atg13 via a TORC1-independent pathway. On the other hand, dephosphorylation of Atg13 was immediately seen upon the addition of ammonium chloride in *pef1Δ* cells (Fig. S2D), indicating that the ability to uptake ammonium chloride in *pef1Δ* cells is intact. Collectively, we found that Pef1 is localized near the vacuole, controls vacuole size and suppresses autophagy through TORC1-dependent and -independent pathways. These findings imply that Pef1 regulates the progression of the sexual differentiation through control of autophagy.

pef1 deletion leads to an imbalance in TORC1 activity

We found that rapamycin sensitivity against autophagy is increased in *pef1Δ* cells (Figs 2D, 3A,D). Similar to our findings, previous comprehensive growth analysis showed that *pef1Δ* cells exhibit a

Journal of Cell Science (2020) 133, jcs247817. doi:10.1242/jcs.247817

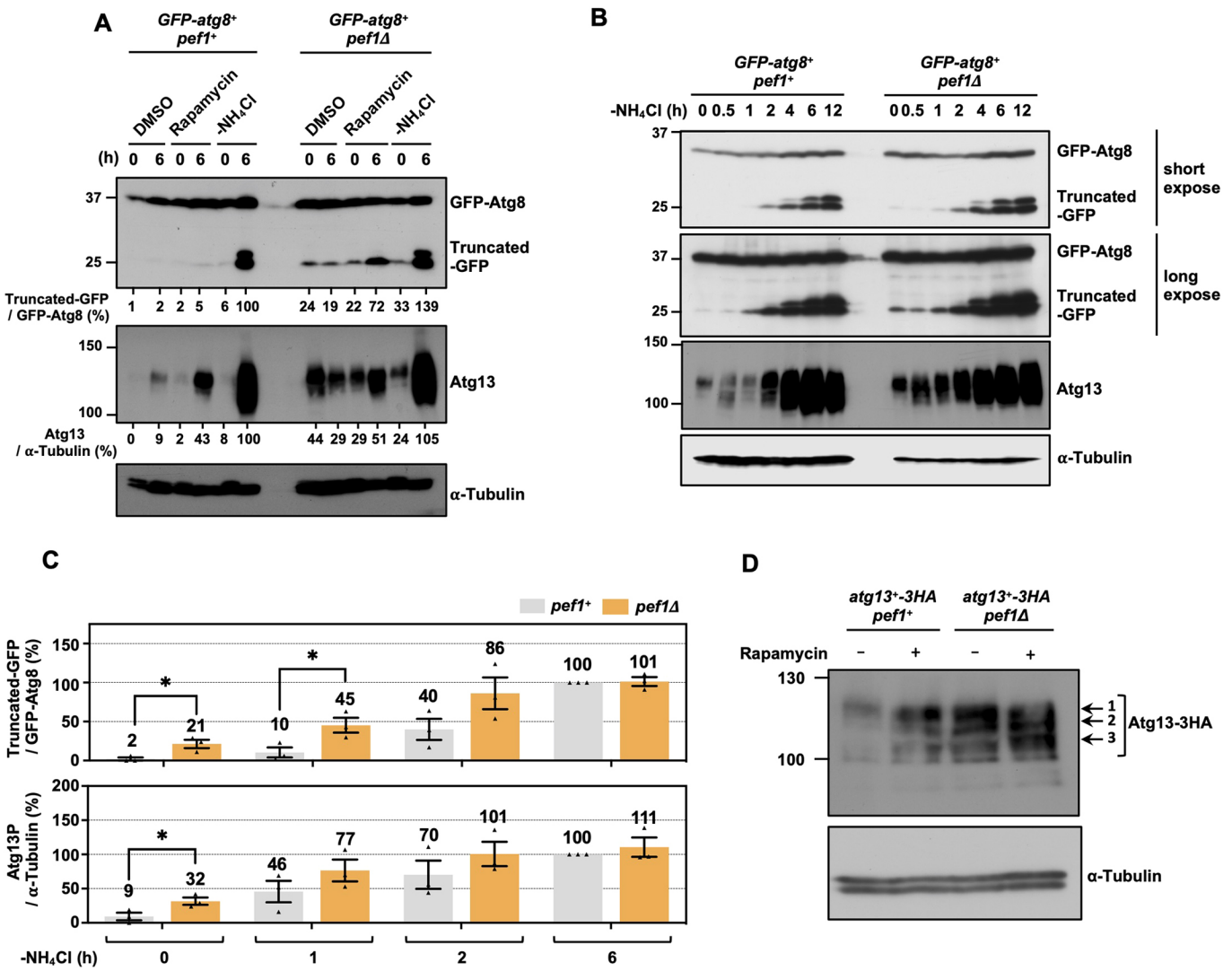

Fig. 3. Pef1 suppresses overactivation of autophagy during the early phase of nitrogen starvation. (A–C) *GFP-atg8*$^{+}$ *pef1*$^{+}$ (JT268) and *pef1Δ* (MS29) strains were incubated in EMM with DMSO or 200 nM rapamycin, or without NH_4Cl for indicated times. The cell extracts were subjected to western blot analysis using mouse anti-GFP, anti-Atg13 or anti-α-tubulin antibodies. The ratio of truncated GFP to GFP–Atg8 and Atg13 to α-tubulin intensities was calculated (C), and presented relative to that at 6 h in *GFP-atg8*$^{+}$ *pef1*$^{+}$, set as 100%. Results are expressed as means±s.e.m. from three independent experiments. *P<0.01 (Student's *t*-tests). (D) *atg13*$^{+}$*-3HA pef1*$^{+}$ (MS1) and *pef1Δ* (MS96) strains were incubated in EMM with DMSO or 200 nM rapamycin for 1 h at 30°C. The cell extracts were subjected to western blot analysis using anti-HA or anti-α-tubulin antibodies. The arrwos at 1, 2 and 3 represent different phosphorylated forms of Atg13–3HA.

slow growth in the presence of rapamycin (Doi et al., 2015). Therefore, we aimed to determine whether rapamycin affects the growth of *pef1Δ* cells. As shown in Fig. 4A, the growth of cells was decreased by *pef1* deletion as compared to control cells (empty vector-expressing *pef1*$^{+}$ strain). In addition, the growth of control cells was unaltered in the presence of rapamycin, but was suppressed by canavanine, a toxic amino acid. By contrast, the growth of *pef1Δ* cells was slightly inhibited by rapamycin, but not by canavanine. This result indicates that the deletion of *pef1* increases rapamycin sensitivity, and resistance to canavanine. Expression of Pef1 (WT, T13A and Y14F) rescued these growth defects back to normal levels, with no differences in growth between these Pef1 mutants. This indicates that the phosphorylation of Thr-13 and Tyr-14 on Pef1 does not affect cell growth. The expression of Pef1 K32R rescued the growth defects of *pef1Δ* cells, but these cells still exhibited rapamycin sensitivity and canavanine resistance. Therefore, we hypothesized that inactivation of Pef1 reduces TORC1 activity and amino acid uptake, and this evidence suggests that the growth defects are due to the loss of Pef1 itself.

To assess whether Pef1 is involved in the regulation of TORC1 activity, we performed western blot analysis to measure phosphorylation levels of Sck1, a substrate of TORC1 (Nakashima et al., 2012). There was less Sck1 phosphorylation in *pef1Δ* cells during the vegetative growth stage (at the point of rapamycin addition, 0 min) as compared with the levels of control cells (Fig. 4B). In the phos-tag gel, the phosphorylation of Sck1 was decreased after treatment with rapamycin for 30 min in control cells, but was rapidly decreased in *pef1Δ* cells after only 15 min. This suggests that Pef1 positively regulates TORC1 activity. We also assessed phosphorylation of Psk1, but we were unable to distinguish the differences in Psk1 phosphorylation between control cells and *pef1Δ* cells during vegetative growth due to strong phosphorylation signals (Fig. 4C, –NH_4Cl 0 h). However, phosphorylation levels of Psk1 at 0.5 to 2 h after nitrogen starvation were below the detection

Journal of Cell Science (2020) 133, jcs247817. doi:10.1242/jcs.247817

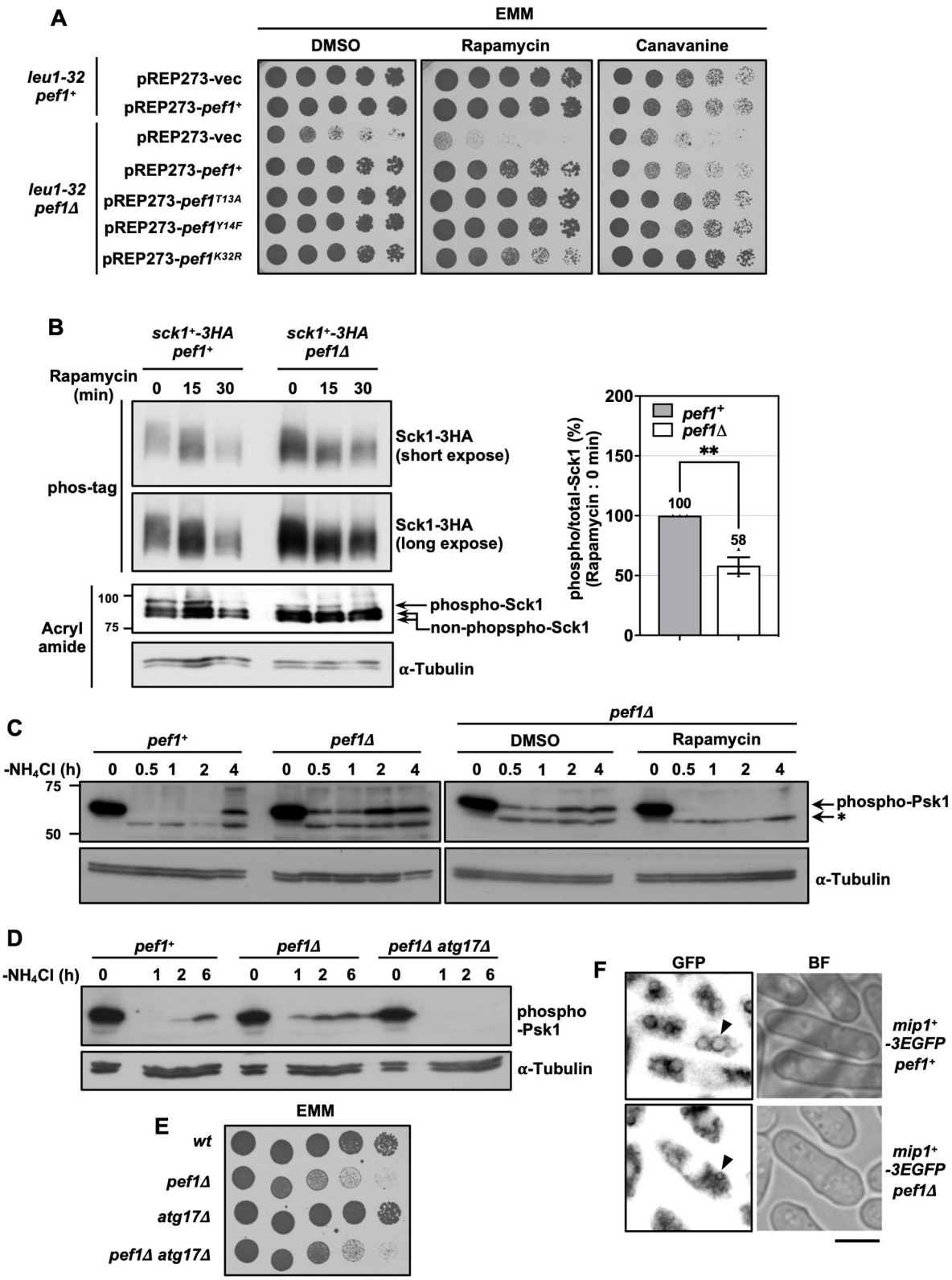

Fig. 4. See next page for legend.

limit in control cells, but were detected at low levels in *pef1Δ* cells (Fig. 4C; Fig. S3A). Phosphorylation of Psk1 in *pef1Δ* cells was ablated by treatment with rapamycin (Fig. 4C), indicating that the low level of phosphorylation of Psk1 was due to activation of TORC1.

To investigate the cause of low TORC1 activity during nitrogen starvation in *pef1Δ* cells, we examined whether autophagy was correlated with low TORC1 activity, as autophagy promotes TORC1 reactivation (Shin and Huh, 2011; Yu et al., 2010). Therefore, we constructed mutants with deletion of both *pef1* and *atg17*, an

Fig. 4. Pef1 regulates balance of TORC1 activity. (A) *leu1-32 pef1*$^{+}$ and *leu1-32 pef1Δ* cells transformed with pREP273 empty vector (MS61 and MS64), *pef1*$^{+}$(MS62 and MS83), *pef1*^{T13A} (MS84), *pef1*^{Y14F} (MS85), *pef1*^{K32R} (MS86) were cultured on EMM containing DMSO, 200 nM rapamycin or 60 µg/ml canavanine for 4 days at 30°C. (B) *sck1*$^{+}$*-3HA pef1*$^{+}$ (AN0150) and *pef1Δ* (MS93) were incubated in EMM with 200 nM rapamycin for the indicated times. The cell extracts were separated by SDS-PAGE using phos-tag or acrylamide gel, and then subjected to western blot analysis using anti-HA or anti-α-tubulin antibodies. The ratio of phosphorylated to total (phospho/total) Sck1 intensities was calculated, and presented relative to the value at 0 min in *sck1*$^{+}$*-3HA pef1*$^{+}$, which was set 100%. Results are expressed as means± s.e.m. from three independent experiments. $^{**}P<0.01$ (Student's *t*-test). (C–E) *pef1*$^{+}$ (L972), *pef1Δ* (MS9), and *pef1Δ atg17Δ* (MS94) cells were incubated in EMM-NH_4Cl with DMSO or 200 nM rapamycin for the indicated times. The cell extracts were subjected to western blot analysis using anti-phospho-p70S6K (Thr-389) and anti-α-tubulin antibodies. Nonspecific bands are indicated with an asterisk (C,D). These cells were also incubated on EMM at 30°C for 3 days (E). (F) *mip1*$^{+}$*-3EGFP pef1*$^{+}$ (AN0494) and *pef1Δ* (MS43) were cultured in EMM. Fluorescence of GFP is shown as gray. Arrowheads highlight the vacuole. Scale bar: 5 µm.

essential gene for autophagy. Western blot analysis confirmed that the TORC1 reactivation was suppressed by the deletion of *atg17* (Fig. S3B). As shown in Fig. 4D, the low Psk1 phosphorylation in *pef1Δ* cells during starvation was abolished in *pef1Δ atg17Δ* cells. However, the growth of *pef1Δ atg17Δ* cells was unaltered as compared with that of *pef1Δ* cells (Fig. 4E). These results indicate that the low TORC1 activity during nitrogen starvation in *pef1Δ* cells is due to excessive autophagy; however, the growth defects of *pef1Δ* cells are not caused by overactivation of autophagy.

Additionally, we examined the intracellular localization of the mammalian raptor ortholog, Mip1. Although *pef1* deletion reduced the size of the vacuole, fluorescence from EGFP-tagged Mip1 was observed at the vacuole membrane in both control and *pef1Δ* cells (Fig. 4F); thus, it appears that Pef1 does not control TORC1 localization. Taken together, these results suggest that Pef1 positively regulates TORC1 activity under nutrient-rich conditions and that Pef1 suppresses the reactivation of TORC1 by blocking excessive autophagy activation during nitrogen starvation.

The double deletion of *pef1* and GATOR1, Rag or Ragulator causes excessive autophagy and TORC1 activation

In order to better understand the interaction of Pef1 and TORC1, we further explored these signaling pathways. Under eutrophic conditions, TORC1 generally promotes cell growth through interactions with its regulators, such as GATOR1, Rag and Ragulator. In *S. pombe*, it has been proposed that Gtr2 (mammalian ortholog RagC and RagD), Lam4 (mammalian ortholog LAMTOR4) and Npr2 (mammalian ortholog NPRL2) are required for maintaining adequate TORC1 activity and normal growth (Chia et al., 2017). Therefore, the disruption of these genes should lead to an imbalance in TORC1 activity, resulting in growth defects. Indeed, as shown in Fig. 5A, we confirmed that *gtr2Δ*, *lam4Δ* and *npr2Δ* cells were unable to grow on yeast extract with supplements (YES) but were able to grow on YES with rapamycin or on EMM. Similarly, *pef1Δ gtr2Δ*, *pef1Δ lam4Δ* and *pef1Δ npr2Δ* cells were not viable on YES but exhibited slow growth on YES with rapamycin and on EMM. The mating ability of *gtr2Δ*, *lam4Δ* and *npr2Δ* cells was significantly decreased on EMM-NH_4Cl agar, and were decreased to moderate levels on SPAS (Fig. 5B). However, the mating ability of *pef1Δ gtr2Δ*, *pef1Δ lam4Δ*, and *pef1Δ npr2Δ* cells was markedly low with both SPAS and EMM-NH_4Cl agar. To validate the effects of these double mutations on TORC1 activity, we examined the phosphorylation levels of Psk1. As shown in Fig. 5C–E, after nitrogen starvation, the Psk1 phosphorylation levels were low in *gtr2Δ*, *lam4Δ* and *npr2Δ cells*, as previously reported (Chia et al., 2017). However, phosphorylation levels were significantly increased in the each double mutant with *pef1* and *gtr2*, *lam4* or *npr2* deletion (Fig. 5C–E; Fig. S3C).

We constructed *GFP-atg8*$^{+}$ *gtr2Δ*, *GFP-atg8*$^{+}$ *lam4Δ*, and *GFP-atg8*$^{+}$ *npr2Δ* mutants to evaluate the levels of autophagy in these strains. During the early phases of nitrogen starvation in *gtr2Δ*, *lam4Δ* and *npr2Δ* cells, the amount of truncated GFP and dephosphorylated Atg13 were increased as compared with the levels in control cells (Fig. 5F–H). Rapamycin treatment did not affect truncated Atg8–GFP, Atg13 phosphorylation and PAS formation in these cells (Fig. 5I,J). Interestingly, high levels of truncated GFP and dephosphorylated Atg13 were detected in *pef1Δ gtr2Δ*, *pef1Δ lam4Δ*, and *pef1Δ npr2Δ* double mutants despite the nutrient rich conditions (Fig. 5F–I). In addition, the amount of truncated GFP and percentage of cells showing PAS formation in these double mutants were substantially increased by rapamycin treatment (Fig. 5I,J; Fig. S4A), indicating that these double mutants are still sensitive to rapamycin treatment. Based on these findings, we hypothesize that the double deletion of *pef1* and *gtr2*, *lam4* or *npr2* causes excessive activation of autophagy, leading to abnormal TORC1 activation and thus blocking the initiation of sexual differentiation. The growth defects in *pef1Δ gtr2Δ*, *pef1Δ lam4Δ*, and *pef1Δ npr2Δ* cells are likely caused by the Pef1 deficit and TORC1 activation. Our results suggest that the GATOR1, Rag and Ragulator complex promotes the activation of TORC1 during the early phases of nitrogen starvation, or blocks excessive activation of autophagy through TORC1-independent pathways.

Evaluation of the effect of double deletion of *pef1* and *tsc1* or *tsc2*

In addition to the GATOR1, Rag and Ragulator complex, the TSC/Rheb pathway is also conserved in *S. pombe* (Chia et al., 2017; Ma et al., 2013; Matsumoto et al., 2002; Murai et al., 2009; Urano et al., 2005, 2007; Uritani et al., 2006; van Slegtenhorst et al., 2004). Notably, previous studies have reported that *pas1*, which encodes the predicted activating subunit of Pef1, genetically interacts with *tsc2*, and is involved in the regulation of amino acid uptake and the G1 arrest of the cell cycle (van Slegtenhorst et al., 2005). Therefore, we hypothesized that *pef1* genetically interacts with *tsc1* or *tsc2*. Using a spot assay to assess resistance to canavanine, we found that *pef1Δ*, *tsc1Δ* and *tsc2Δ* cells all displayed resistance (Fig. 6A). Additionally, the *pef1Δ tsc1Δ* and *pef1Δ tsc2Δ* double mutants exhibited slow growth, rapamycin sensitivity and canavanine resistance to a similar extent to that found in *pef1Δ* cells. Mating efficiencies of *tsc2Δ* cells and *pef1Δ tsc2Δ* cells, as well as *pef1Δ* cells, were also significantly decreased on EMM-NH_4Cl agar as compared with SPAS (Fig. 6B). These findings suggest that the Pef1 and TSC complex are components of the same signaling pathway, as there were no differences between the *pef1Δ* and double mutants under these different conditions.

We next examined the effect on TORC1 activity in *tsc1Δ* and *tsc2Δ* cells. As shown in Fig. 6C,D, neither *tsc1Δ* nor *tsc2Δ* cells had decreased Psk1 phosphorylation under starvation conditions. Additionally, *pef1Δ tsc1Δ* and *pef1Δ tsc2Δ* cells were unable to attenuate Psk1 phosphorylation during starvation, with phosphorylation levels of the same intensity as *tsc1Δ* and *tsc2Δ* cells, respectively. These results suggest that *tsc2* has a stronger genetic interaction with TORC1 than Pef1. In contrast, the amount of degraded GFP–Atg8 induced by nitrogen starvation was no different between control, *tsc1Δ* cells, and *tsc2Δ* cells, but that

Journal of Cell Science (2020) 133, jcs247817. doi:10.1242/jcs.247817

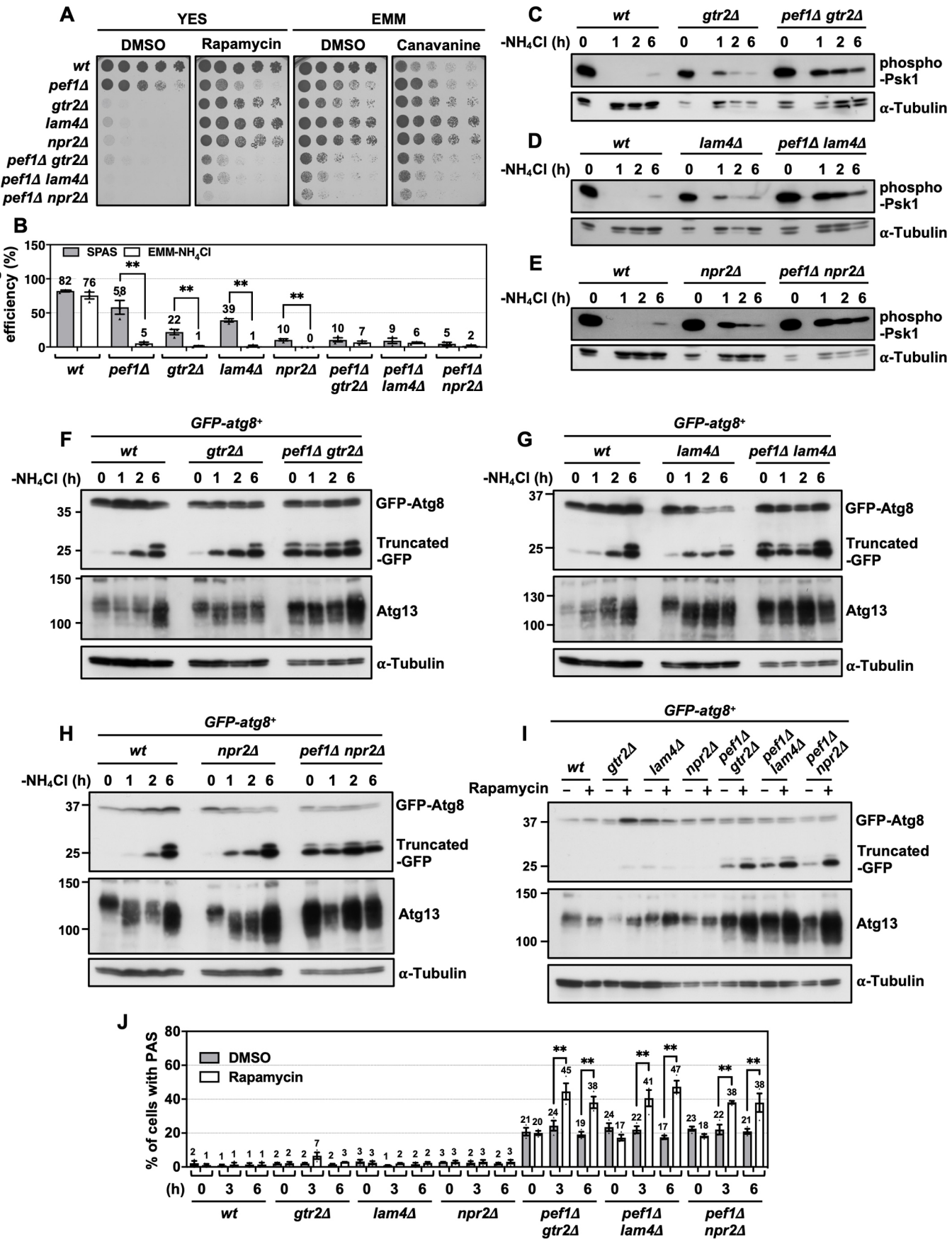

Fig. 5. See next page for legend.

Journal of Cell Science (2020) 133, jcs247817. doi:10.1242/jcs.247817

Fig. 5. Double deletion of *pef1* and components of the GATOR1, Rag and Ragulator pathway affect growth, mating efficiency and autophagy. (A) *wt* (972), *pef1Δ* (MS9), *gtr2Δ* (MO11), *lam4Δ* (MO6), *npr2Δ* (YM15), *pef1Δ gtr2Δ* (MS203), *pef1Δ lam4Δ* (MS185), and *pef1Δ npr2Δ* (MS205) cells were cultured on YES with DMSO or 200 nM rapamycin for 2.5 days at 30°C. These cells were also cultured on EMM with or without 60 µg/ml canavanine for 4.5 days at 30°C. (B) *wt* (968), *pef1Δ* (MS8), *gtr2Δ* (MO13), *lam4Δ* (MO7), *npr2Δ* (YM25), *pef1Δ gtr2Δ* (MS204), *pef1Δ lam4Δ* (MS186), and *pef1Δ npr2Δ* (MS206) were incubated on SPAS or EMM-NH_4Cl for 2 days at 25°C. The fixed cells were stained with DAPI, and observed using fluorescence microscopy to determine mating efficiency. Results are expressed as means±s.e.m. from three independent experiments (at least 100 cells were counted for each genotype and condition). ***P*<0.01 (Student's *t*-test). (C–E) The strains used in A were incubated in EMM-NH_4Cl for the indicated times. The cell extracts were subjected to western blot analysis using anti-phospho-p70S6K (Thr-389) and anti-α-tubulin antibodies. (F–J) *GFP-atg8*$^+$ *wt* (JT268), *gtr2Δ* (MS174), *lam4Δ* (MS175), *npr2Δ* (MS177), *pef1Δ gtr2Δ* (MS187), *pef1Δ lam4Δ* (MS183) and *pef1Δ npr2Δ* (MS191) cells were incubated in EMM-NH_4Cl for the indicated times (F–H). These strains were also incubated in EMM with DMSO or 200 nM rapamycin for 3 h at 30°C (I). The cell extracts were subjected to western blot analysis using mouse anti-GFP, anti-Atg13, or anti-α-tubulin antibodies (F–I). These cells were also incubated in EMM with DMSO or 200 nM rapamycin for the indicated times. (J) Percentages of cells with PAS were are expressed as means±s.e.m. from three independent experiments (at least 100 cells were counted for each genotype and condition). ***P*<0.01 (Student's *t*-test).

rapidly increased in *pef1Δ tsc1Δ* cells and *pef1Δ tsc2Δ* cells to the same level as *pef1Δ* cells (Fig. 6E,F). Rapamycin treatment increased levels of autophagy in both *pef1Δ tsc1Δ* cells and *pef1Δ tsc2Δ* cells to the same level as *pef1Δ* cells, but levels of autophagy remained unaltered in *tsc1Δ* cells and *tsc2Δ* cells (Fig. 6G,H; Fig. S4B). Therefore, *pef1* might have a stronger genetic interaction with regards to autophagy regulation than *tsc1* and *tsc2*. Therefore, Pef1 may positively regulate TORC1 via Tsc1 and Tsc2 but may regulate autophagy through a TSC-TORC1-independent pathway.

Pef1 physically interacts with Clg1, Pas1 and Psl1

Although these results provide insight to the pathways downstream from Pef1, little is known about the signaling pathways upstream of Pef1 that are involved in sexual differentiation. Previous studies have suggested that Pef1 physically interacts with the three cyclins Clg1, Pas1 and Psl1 (Chen et al., 2013; Tanaka and Okayama, 2000). However, basic information on the expression pattern, the intracellular localization and the stoichiometry of interactions between Pef1 and these cyclins remain unclear. To confirm interactions between Pef1 and these cyclins, we performed immunoprecipitation. As shown in Fig. 7A, a band for Psl1–GFP near 50 kDa and subtle band for Clg1–GFP near 75 kDa were detected in the Myc-eluted solutions from cells expressing Pef1–13myc, but the Pas1–GFP signal was below the detection limit. Additionally, a Pef1–13myc band near 63 kDa was clearly detected in the Clg1–GFP and Psl1–GFP immunoprecipitants, but was undetected in the GFP immunoprecipitate of Pas1–GFP. Based on these findings, we hypothesize that the interaction of Pef1 and Psl1 is stronger than that of Pef1 and Clg1. We also observed that Pef1–GFP and Psl1–RFP were colocalized in the nucleus, and Clg1–GFP and Pas1–RFP appeared to be colocalized with Pef1–GFP in the cytoplasm (Fig. 7B); however, Pas1–RFP signals were very weak.

We next examined the effects of nitrogen starvation on the interactions between Pef1 and cyclins. To this end, we used the *pef1*$^+$*-3HA pas1*$^+$*-13myc* strain because Pas1–GFP was undetectable. As shown in Fig. 7C–F, Pef1–13myc and Psl1–GFP were consistently expressed after nitrogen starvation, whereas expression of Clg1–GFP and Pas1–13myc were decreased after nitrogen starvation. Interaction intensities between Pef1 with both Clg1 and Pas1 were also decreased by nitrogen starvation (Fig. 7G,H), but Psl1 stably interacted with Pef1 after nitrogen starvation (Fig. 7I). Taken together, these results suggest that Pef1 interacts with Clg1 and Pas1 in the cytoplasm, and with Psl1 in the nucleus. Nitrogen starvation decreased the intensity of Pef1–Clg1 and Pef1–Pas1 interaction complexes, but not that of the Pef1–Psl1 complex. Therefore we hypothesize that Clg1 and Pas1 play a role in the nitrogen starvation response.

Clg1 and Pas1 are activators of Pef1 in regulation of TORC1 and autophagy

To validate the genetic interaction between *pef1* and these cyclins, we constructed a series of cyclin-deleted mutants. In Fig. 8A, a spot assay showed that single deletion of *clg1*, *pas1* and *psl1* does not affect the growth, while double mutants with *pef1* and cyclin deletion have a decreased growth response on YES to the same level as that of *pef1Δ* cells. However, the growth of *pef1Δ clg1Δ* cells on EMM was lower than that of *pef1Δ* cells, suggesting that *clg1* deletion may affect growth through a *pef1*-independent pathway in the case of EMM condition. In the double or triple mutants with deletion of cyclins, *clg1Δ psl1Δ* and *pas1Δ psl1Δ* cells normally grew; however, *clg1Δ pasl1Δ* cells grew at the same rate as *pef1Δ* cells. These results indicate that the growth defect is caused by loss of interactions between Pef1, Clg1 and Pas1.

We also examined the mating efficiency of cyclin-deficient mutants (Fig. 8B). The mating ability of *psl1Δ* cells on EMM-NH_4Cl agar was significantly decreased when compared with the mating ability on SPAS; however, *pas1Δ* cells had no differences in mating efficiency between SPAS and EMM-NH_4Cl agar. Additionally, the mating efficiency of *clg1Δ* cells was significantly lower on both SPAS and EMM-NH_4Cl agar than that of wild-type cells but was restored by the double deletion *clg1Δ pas1Δ*. These results suggest that the mating process is promoted by Clg1 and Psl1 and suppressed by Pas1.

In order to assess whether these cyclins genetically interact with TORC1 signaling, we assessed Psk1 phosphorylation with single deletion of *clg1*, *pas1* or *psl1*. In these mutants, the Psk1 phosphorylation levels after nitrogen starvation were similar to those of wild-type cells (Fig. S5A–C). However, the Psk1 phosphorylation levels in *clg1Δ pas1Δ* cells and *clg1Δ pas1Δ psl1Δ* cells remained high after nitrogen starvation (Fig. 8C, Fig. S5G), but other double mutants (*clg1Δ psl1Δ* and *pas1Δ psl1Δ*) had no differences in the levels of phosphorylation as compared to wild-type cells (Fig. S5E,F). Although *clg1Δ pas1Δ* cells maintained low Psk1 phosphorylation levels during nitrogen starvation, its phosphorylation levels were higher than those of *pef1Δ* cells. This suggests that Clg1 and Pas1 may also control TORC1 signaling through a Pef1-dependent and -independent pathway.

We also measured levels of autophagy by assessing truncated GFP during nitrogen starvation, and observed no differences between single mutants (*clg1Δ*, *pas1Δ*, *psl1Δ*) and wild-type cells (Fig. S5H). However, *clg1Δ pas1Δ* cells had high levels of autophagy during nitrogen starvation, comparable to the levels in *pef1Δ* cells (Fig. 8D; Fig. S6A,B) and after rapamycin stimulation (Fig. 8E; Fig. S7A,B). Vacuole size in *clg1Δ pas1Δ* cells was also reduced, similar to what is seen in *pef1Δ* cells (Fig. S8). These results suggest that Clg1 and Pas1 regulate both autophagy and TORC1. Taken together, these analyses indicate that Clg1 and Pas1 are activators of Pef1 in the regulation of TORC1 and autophagy. In contrast, the Pef1–Psl1 complex likely controls the initiation of the mating process through a distinct pathway separate from TORC1 and autophagy, such as a meiosis-related signaling pathway.

Journal of Cell Science (2020) 133, jcs247817. doi:10.1242/jcs.247817

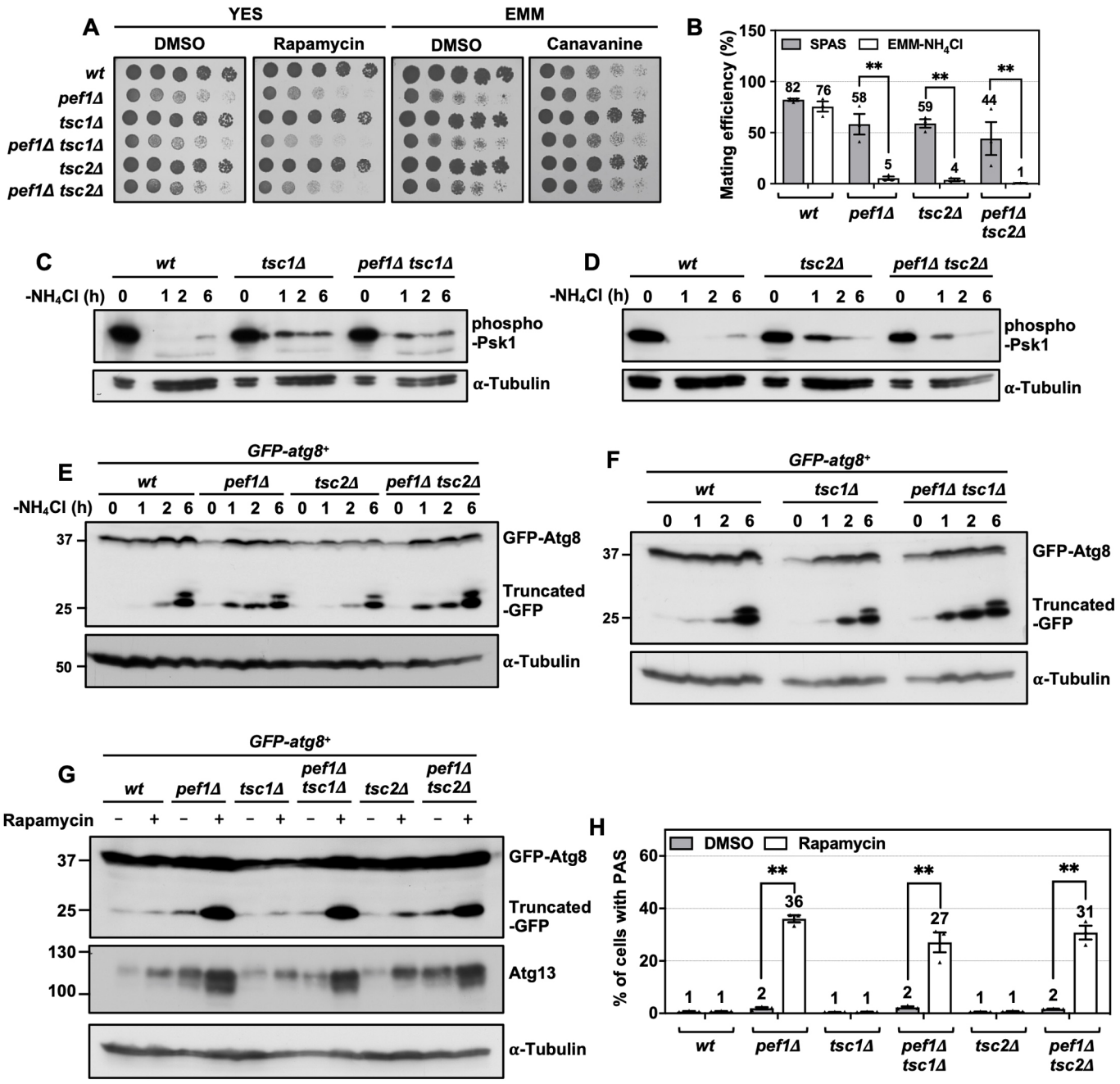

Fig. 6. *pef1* genetically interacts with *tsc1* and *tsc2*. (A) *wt* (972), *pef1Δ* (MS9), *tsc1Δ* (AN0777), *pef1Δ tsc1Δ* (MS218), *tsc2Δ* (JU1355), and *pef1Δ tsc2Δ* (MS147) were cultured on YES containing DMSO or 200 nM rapamycin for 2.5 days at 30°C. These cells were also cultured on EMM with or without 60 µg/ml canavanine for 4.5 days at 30°C. (B) *tsc2Δ* (AN0781), and *pef1Δ tsc2Δ* (MS148) were incubated on SPAS or EMM-NH_4Cl agar for 2 days at 25°C. Then, the cells were fixed and stained with DAPI, and observed using fluorescence microscopy to determine mating efficiency. For comparison, the mating efficiency of *wt* (968) and *pef1Δ* (MS8) shown in Fig. 5B is re-plotted. Results are expressed as means±s.e.m. from three independent experiments (at least 100 cells were counted for each genotype and medium condition). $^{**}P<0.01$ (Student's *t*-test). (C,D) The strains used in A were incubated in EMM-NH_4Cl for the indicated times. The cell extracts were subjected to western blot analysis using anti-phospho-p70S6K (Thr-389) or anti-α-tubulin antibodies. (E–H) *GFP-atg8*$^+$ *wt* (JT268), *tsc2Δ* (MS151), *pef1Δ tsc2Δ* (MS149), *tsc1Δ* (MS217), and *pef1Δ tsc1Δ* (MS219) cells were incubated in EMM-NH_4Cl for the indicated times (E,F). These cells were also incubated in EMM with DMSO or 200 nM rapamycin for 3 h (G,H). The cell extracts were analyzed by western blotting using mouse anti-GFP, anti-Atg13 or anti-α-tubulin antibodies (E–G). (H) Percentages of cells with PAS are expressed as means±s.e.m. from three independent experiments (at least 100 cells were counted for each genotype and medium condition). $^{**}P<0.01$ (Student's *t*-test).

DISCUSSION

Pef1 was originally identified as a kinase that contains a PSTAIRE motif, which is a highly conserved amino acid sequence of the CDK family (Tournier et al., 1997). There have been few studies that aimed to identify the function, activation mechanisms and downstream pathways of Pef1. In this study, we revealed that Pef1 regulates the initiation of sexual differentiation through controlling TORC1 activity, autophagy and the Ste11-Mei2 pathway (Fig. 8F). The deletion of *pef1* decreased TORC1 activity toward Sck1 and increased autophagy activity in the nutrient-rich condition. In

Journal of Cell Science (2020) 133, jcs247817. doi:10.1242/jcs.247817

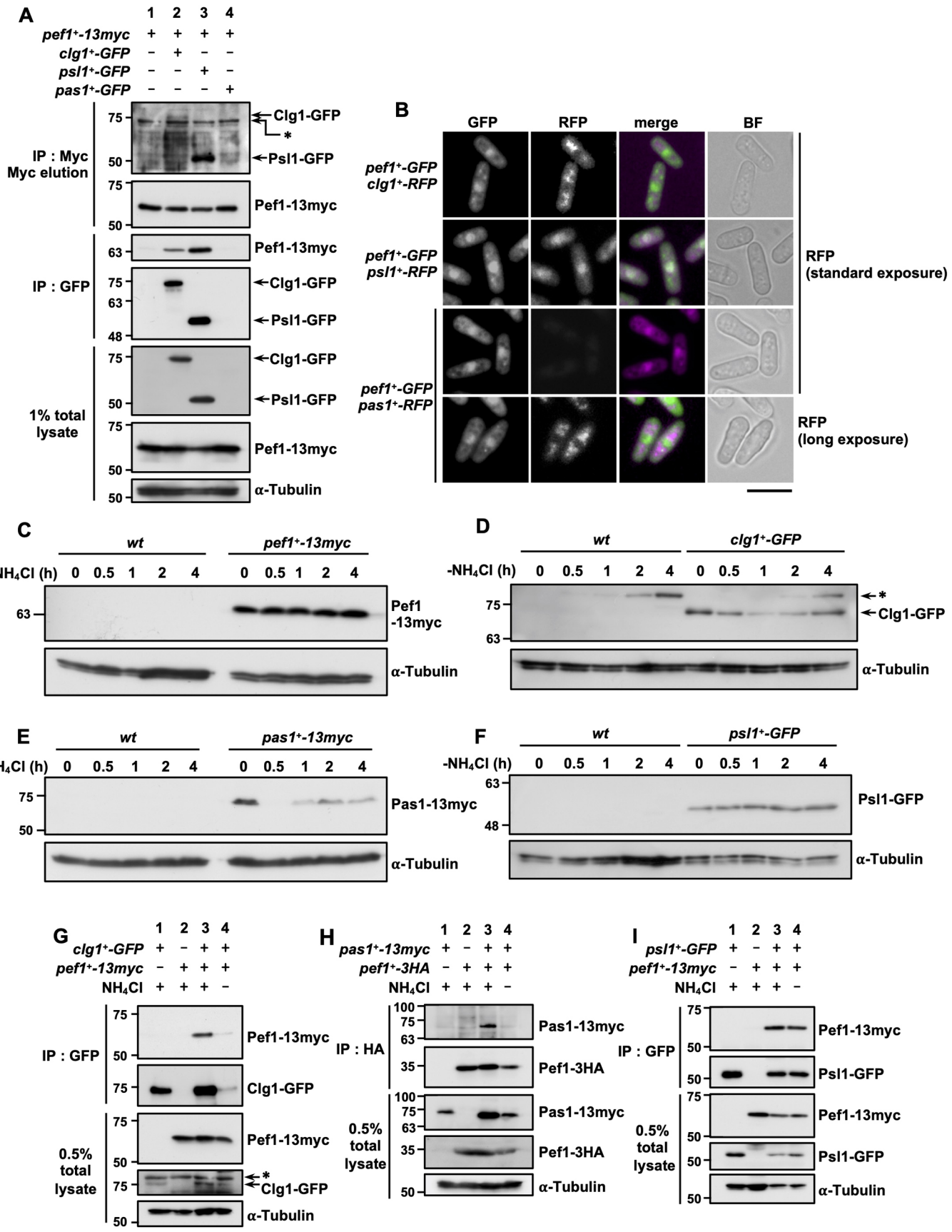

Fig. 7. See next page for legend.

Fig. 7. Pef1 physically interacts with Clg1, Pas1 and Psl1. (A) *pef1*$^{+}$*-13myc* (MS49, lane 1), *pef1*$^{+}$*-13myc clg1-GFP* (MS216, lane 2), *pef1*$^{+}$*-13myc psl1-GFP* (MS213, lane 3) and *pef1*$^{+}$*-13myc pas1-GFP* (MS211, lane 4) cells were exponentially grown in EMM. The cell extracts were subjected to immunoprecipitation (IP) using anti-Myc or rabbit anti-GFP antibodies. Both of 1% volume of cell lysates and immunoprecipitants were analyzed by western blotting using anti-Myc, mouse anti-GFP or anti-α-tubulin antibodies. Nonspecific bands are indicated with an asterisk. (B) *pef1*$^{+}$*-GFP clg1*$^{+}$*-RFP* (MS161), *pef1*$^{+}$*-GFP pas1*$^{+}$*-RFP* (MS165), and *pef1*$^{+}$*-GFP psl1*$^{+}$*-RFP* (MS163) were incubated in EMM. Fluorescence of Pef1–GFP is shown as green. Clg1–RFP, Pas1–RFP and Psl1–RFP are shown as magenta. Merge images are white. Scale bar: 10 µm. (C–F) *wt* (L972), *pef1*$^{+}$*-13myc* (MS49), *clg1*$^{+}$*-GFP* (MS131), *pas1*$^{+}$*-13myc* (MS227) and *psl1*$^{+}$*-GFP* (MS135) cells were incubated in EMM-NH_4Cl for indicated times. The cell extracts were subjected to western blot analysis using anti-Myc, mouse anti-GFP or anti-α-tubulin antibodies. Nonspecific bands are indicated with an asterisk. (G–I) *clg1*$^{+}$*-GFP* (MS131, lane 1 of G), *pas1*$^{+}$*-13myc* (MS227, lane 1 of H), *psl1*$^{+}$*-GFP* (MS135, lane 1 of I), *pef1*$^{+}$*-13myc* (MS49, lane 2 of G,I), *pef1*$^{+}$*-3HA* (MS47, lane 2 of H), *pef1*$^{+}$*-13myc clg1*$^{+}$*-GFP* (MS216, lanes 3 and 4 of G), *pef1*$^{+}$*-3HA pas1*$^{+}$*-13myc* (MS245, lanes 3 and 4 of H), and *pef1*$^{+}$*-13myc psl1*$^{+}$*-GFP* (MS213, lanes 3 and 4 of I) were incubated in fresh EMM (NH_4Cl: +) or EMM-NH_4Cl (NH_4Cl : –) for 1 h. The cell extracts were immunoprecipitated with rabbit anti-GFP antibody (G,I) or anti-HA Affinity Matrix (H). Immunoprecipitants and cell extracts were subjected to western blot analysis using anti-Myc, mouse anti-GFP, anti-HA or anti-α-tubulin antibodies. Nonspecific protein bands are indicated with an asterisk.

addition, the TORC1 reactivation induced by autophagy was promoted in *pef1Δ* cells during the early phase of nitrogen starvation. Thus, we predict that *pef1* regulates the initiation of sexual differentiation through control of the balance between the TORC1 signaling pathway and autophagy.

To obtain a clue for the mechanism of the Pef1-TORC1 signaling pathway, we examined the genetic interaction between *pef1* and TORC1 regulators. We found that the double deletion of *pef1* and components of the GATOR1, Rag and Ragulator pathway causes excessive autophagy and TORC1 reactivation after nitrogen starvation. In mammals, nucleotide-bound Rags (RagA/B-GTP or RagC/D-GDP) tether TORC1 to the lysosomal membrane, where TORC1 is subsequently activated by the TSC/Rheb signaling pathway (Saxton and Sabatini, 2017). Although the deletion of GATOR1, Rag or Ragulator components in *S. pombe* did not alter the localization of Mip1, cells lacking these components were not viable in YES (Chia et al., 2017). Chia et al. also observed severe growth defects on YES when the wild-type Gtr1 (the counterpart of mammalian RagA/B) is artificially mutated so that it is locked in GTP-bound form (Gtr1 Q61L). Thus, it is hypothesized that GATOR1, Rag and the Ragulator complex suppresses TORC1 activity to maintain growth homeostasis in *S. pombe*. In contrast, we noticed that deletion of *gtr2*, *lam4* or *npr2* promoted autophagy during the early phases of nitrogen starvation, suggesting that these components possibly enhance TORC1 activity or suppress autophagy via a TORC1-independent manner. Therefore, simultaneous evaluation of the several TORC1 downstream pathways or cellular responses is necessary to reveal the true function of the GATOR1, Rag and Ragulator complex pathway in *S. pombe.*

The TSC complex is comprised of two proteins, hamartin and tuberin, which are products of the tuberous sclerosis genes *tsc1* and *tsc2*. This complex serves as the GAP for the small G protein Rheb (Huang and Manning, 2008; Saxton and Sabatini, 2017). The mammalian TSC complex plays a critical role as the signal integrator of TORC1 regulation, and is important for sensing nutrition, growth factors and stress. TSC1 and TSC2 are the targets of various kinases, such as Akt, ERK and AMPK (Huang and Manning, 2008). CDK1–cyclin B also phosphorylates Thr-417, Ser-584, and Thr-1047 of TSC1 during the G2/M phase of the cell cycle in HEK293 cells, and phosphorylation of these sites leads to the inhibition of TSC complex activity (Astrinidis et al., 2003). Additionally, quantitative proteomic analysis indicates that Ser-862 of Tsc1 in *S. pombe*, which contains the CDK phosphorylation motif Ser-Thr-Pro, is phosphorylated during mitosis (Swaffer et al., 2018). This suggests that CDKs, including Pef1, in *S. pombe* regulate the activity of the TSC complex through direct phosphorylation of Tsc1. Alternative reports suggest that the deletion of *tsc2* increases the expression of cyclin Pas1 (van Slegtenhorst et al., 2005). Therefore, the Pef1–Pas1 complex may create a positive or negative feedback loop via Tsc1 and Tsc2 to control TORC1 activity.

We also found that Pef1 is involved in the regulation of expression of Ste11 during nitrogen starvation (Fig. 1C,E,F). Ste11 plays an important role for upregulating various gene sets related to conjugation and initiation of meiosis, such as *mei2* (Mata and Bähler, 2006; Sugimoto et al., 1991). Ste11 expression and activity are controlled by multiple pathways including mating pheromones, nutrition and stress (Anandhakumar et al., 2013; Otsubo and Yamamoto, 2012). For instance, the cAMP/PKA pathway suppresses the transcription of *ste11* mRNA via direct inhibition of the zinc-finger transcription factor Rst2 (Higuchi et al., 2002; Kunitomo et al., 2000). The expression of Ste11 was increased in response to nitrogen starvation, but was suppressed by *pef1* deletion. *pef1* deletion also promoted the reactivation of TORC1. Therefore, we hypothesized that Pef1 upregulates expression of Ste11 through suppression of the TORC1 pathway; however, the Ste11-Mei2 pathway was strongly silenced in *pef1Δ* cells. This indicates that cAMP/PKA or another Ste11 regulatory pathway may also be impaired by *pef1* gene disruption. Interestingly, mammalian PKA directly phosphorylates CDK16 and CDK18 (Graeser et al., 2002; Matsuda et al., 2014), which leads to alterations of their activities. Thus, Pef1 controls Ste11 through not only TORC1, but also via cAMP/PKA or other kinases, such as Pat1, Spk1 or Cdc2 (Anandhakumar et al., 2013; Otsubo and Yamamoto, 2012).

Nitrogen starvation induces G1 arrest of the cell cycle, but the relationship between TORC1 signaling and the cell cycle machinery remained unclear. Recent studies have investigated the great wall kinase (Gwl)/endosulfin/PP2A/B55 pathways. Gwl directly phosphorylates endosulfin, and phosphorylated endosulfin associates with the phosphatase PP2A to inhibit PP2A activity, thus, resulting in activation of CDK1–cyclin B (Pérez-Hidalgo and Moreno, 2017). *S. pombe* contains three Gwl ortholog genes, *ppk18*, *cek1* and *ppk31* (Aono et al., 2019). The Ppk18-Igo1 (*S. pombe* endosulfin) pathway is also negatively regulated by the TORC1-Sck2 pathway, resulting in the activation of PP2A, which promotes the cell cycle (Chica et al., 2016; Pérez-Hidalgo and Moreno, 2017). Interestingly, previous reports have suggested that Pef1 physically interacts with the Gwl orthologs Cek1 and Ppk18 to control chronological life span (Chen et al., 2013); however, this relationship and the molecular mechanisms are poorly understood. Notably, Cek1, Ppk18 and Ppk31 contain many CDK phosphorylation motifs, Ser-Thr-Pro, in their amino acid sequences (Cek1, 20 sites; Ppk18, 21 sites; Ppk31, 4 sites). As the direct connection between CDK and Gwl is conserved among budding yeast, *Xenopus* and humans, it is possible that Pef1 controls the TORC1 pathway through direct phosphorylation of Gwl.

CDK activity typically oscillates during the cell cycle via switching of their regulatory subunits, phosphorylation or binding to CDK inhibitors (Malumbres and Barbacid, 2005). Mammalian

Journal of Cell Science (2020) 133, jcs247817. doi:10.1242/jcs.247817

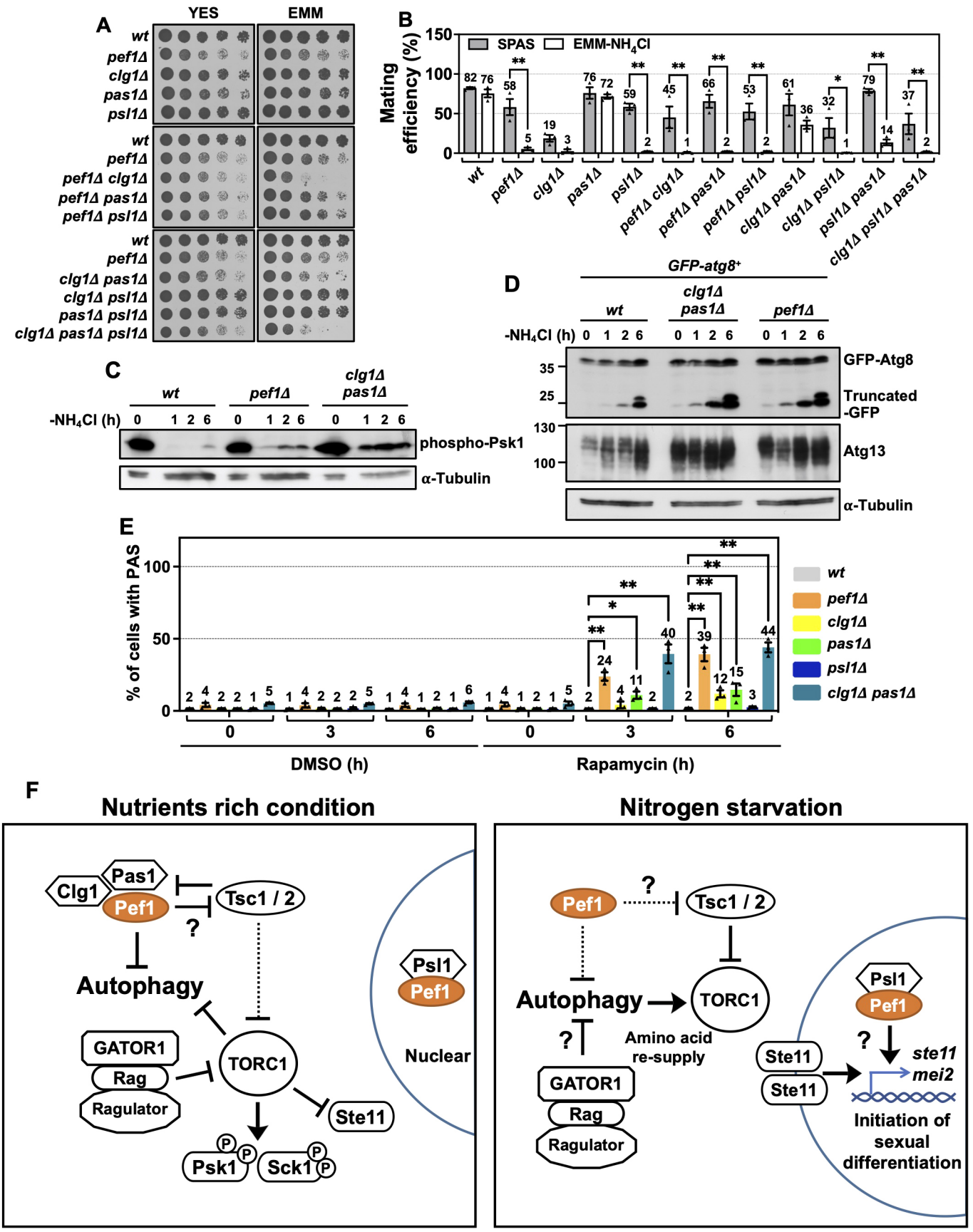

Fig. 8. See next page for legend.

Fig. 8. Double deletion of *clg1* and *pas1* induces activation of TORC1 and autophagy during the early phase of nitrogen starvation. (A,B) *wt* (A, 972), *pef1Δ* (A, MS9), *clg1Δ* (A, MS67; B, MS68), *pas1Δ* (A, MS69; B, MS70), *psl1Δ* (A, MS65; B, MS66), *pef1Δ clg1Δ* (A, MS76; B, MS78), *pef1Δ pas1Δ* (A, MS77; B, MS79), *pef1Δ psl1Δ* (A, MS74; B, MS75), *clg1Δ pas1Δ* (A, MS159; B, MS160), *clg1Δ psl1Δ* (A, MS157; B, MS158), *pas1Δ psl1Δ* (A, MS113; B, MS114), and *clg1Δ pas1Δ psl1Δ* (A, MS115; B, MS116) cells were cultured on YES or EMM for 2–5 days at 30°C (A), SPAS or EMM-NH_4Cl for 2 days at 25°C (B), respectively. The fixed cells were stained with DAPI and subsequently observed using fluorescence microscopy to determine mating efficiency. For comparison, the mating efficiency of *wt* (968) and *pef1Δ* (MS8) shown in Fig. 5B is re-plotted. Results are expressed as means±s.e.m. from three independent experiments (at least 100 cells were counted for each genotype and condition). **P*<0.05, ***P*<0.01 (Student's *t*-test). (C) *wt* (972), *pef1Δ* (MS9), and *clg1Δ pas1Δ* (MS159) were incubated in EMM-NH_4Cl for indicated times, and then these cells were fixed. The cell extracts were subjected to western blot analysis using anti-phospho-p70S6K (Thr-389) or anti-α-tubulin antibodies. (D,E) *GFP-atg8*$^+$ *wt* (JT268), *pef1Δ* (MS29), *clg1Δ* (MS102), *pas1Δ* (MS103), *psl1Δ* (MS104) and *clg1Δ pas1Δ* (MS202) cells were incubated in EMM-NH_4Cl for indicated times. The cell extracts were subjected to western blot analysis using mouse anti-GFP, anti-Atg13 or anti-α-tubulin antibodies (D). These cells were also incubated in EMM with DMSO or 200 nM rapamycin for indicated times. (E) Percentages of cells with PAS are expressed as mean±s.e.m. from three independent experiments (at least 100 cells were counted for each genotype and condition). **P*<0.05, ***P*<0.01 (one-way ANOVA). (F) The predicted signaling pathway of Pef1 in the initiation of sexual differentiation. See Discussion for further details.

CDK5 and budding yeast PHO85 also cooperate with their interacting partner to exert their physiological functions in response to environmental changes, such as neural differentiation or various stressors (Dhavan and Tsai, 2001; Huang et al., 2007). In budding yeast, ten cyclins have been identified as PHO85 partners, known as PHO85 cyclins (PCLs). Each PCL–PHO85 complex targets different substrates, resulting in the induction of multi-spectral cell responses including growth, alterations in cell morphology or the sensing of stress (Huang et al., 2007). Our data suggests that Pef1 also changes its interacting partner in response to nutrient conditions, as Pas1 and Clg1 dissociated from Pef1 during nitrogen starvation. Additionally, the double deletion of *pas1* and *clg1* caused similar growth, autophagy and TORC1 activity phenotypes to those of *pef1Δ* cells. Thus, we predict that the Pef1–Clg1 and Pef1–Pas1 complexes control TORC1 and autophagy. In contrast, *psl1Δ* cells showed no mating ability on EMM-NH_4Cl agar similar to *pef1Δ* cells, and Psl1 stably interacted with Pef1 in the nucleus despite nitrogen starvation conditions. This implies that the Pef1–Psl1 complex controls nuclear-specific functions, such as meiosis progression, transcription or DNA repair. Alternately, it is expected that each *S. pombe* Pef1–cyclin complex targets different substrates in response to altered environmental conditions, similar to PCL–PHO85 complexes in *S. cerevisiae*. The deletion of *pas1* may alter the activity of Cdc2, as previous studies suggest that Pas1 preferentially interacts with Cdc2 over Pef1 (Tanaka and Okayama, 2000). Therefore, we hypothesize that the growth defects in *pef1Δ* cells may be due to activation of Cdc2, as *pef1* deletion may lead to increases in the levels of free Pas1. If so, further studies investigating how the expression ratio of Pef1:Cdc2 influences the cell cycle control would be of interest.

This study provides insight into the activation mechanisms and downstream signaling pathways of Pef1. As Pef1 is a member of the conserved CDK5 subfamily, elucidating its relationship with TORC1 could contribute a better understanding and these pathways and potential drug targets for a variety of human disorders including cancer, metabolic syndrome and neurodegenerative diseases. In order to develop a better understanding of the physiological functions of Pef1, future studies should incorporate proteomic and genomic techniques to identify substrates, activators or inhibitors of Pef1.

MATERIALS AND METHODS

Yeast strains, growth conditions and general methods

S. pombe strains used in this study are listed in Table S1. The cells were precultured on yeast extract with supplements (YES) or Edinburgh minimal medium (EMM), which contained 20 mg/ml glucose as a carbon source and 500 µg/ml ammonium chloride as a nitrogen source (Moreno et al., 1991). Before experiments, the cells were grown in EMM under shaking at 90 rpm at 25–30°C until they reached an optical density at 595 nm (OD_{595}) of 0.6–0.8. EMM-NH_4Cl, a nitrogen-free medium, was used for the starvation experiments. For spot assays, 6 µl of five-times serially diluted cultures were spotted on each medium and incubated for 2–4 days at 30°C. Rapamycin (Calbiochem) and canavanine (Sigma) were used at a final concentration of 200 nM and 60 µg/ml, respectively. For mating and sporulation, cells were cultured on sporulation agar with supplements (SPAS), which contained 45 mg/l adenine, leucine, uracil, histidine and lysine as amino acid sources, or EMM-NH_4Cl agar at 25°C for 2 days (Sabatinos and Forsburg, 2010). General and molecular genetic techniques followed standard protocols (Moreno et al., 1991; Okazaki et al., 1990; Sabatinos and Forsburg, 2010).

Construction of modified strains and gene expression plasmids

Direct chromosomal integration methods were used to integrate 3HA-hphMX, 13myc-hphMX, GFP-hphMX, or RFP-kanMX cassettes before terminal codons of the *pef1*, *clg1*, *pas1* and *psl1* genes. Gene disruptions were performed by replacing individual open reading frames (ORFs) with kanMX, hphMX or natMX cassettes (Bähler et al., 1998; Sato et al., 2005). To construct *pef1*$^+$ expression plasmids, the cDNA encoding full-length *pef1*$^+$ was cloned by PCR using a cDNA library (NBRP) and specific primers with restriction site sequences of NotI and SmaI at their 5′ end (lowercase), respectively (forward primer, 5′-gcactatgcggccgcATGAACTACCAAAGGCTT-3′; reverse primer, 5′-gcacttcccgggCTATGCGGTTAAAAACCAAGC-3′). The PCR product was subcloned into pREP273-3HA vector (Nakashima et al., 2014), which was generated by the replacement of multi-cloning sites together with the *nmt41* promoter (Basi et al., 1993) and 3HA fragment from pSLF273 (NBRP). Point mutations of Pef1 were introduced by site-directed mutagenesis. To construct a *tor2*$^+$ expressing vector, a PCR product, which consisted of *tor2*$^+$ ORF and 1000 bp of its 5′ and 3′ flanking regions, was inserted into pAL-KS- vector using the infusion cloning method.

Protein preparation, immunoprecipitation and immunoblotting

Cell cultures were mixed with 7% trichloroacetic acid, put on ice for at least 10 min, and then centrifuged (3300 rpm for 5 min). Cell pellets were washed twice with cold acetone and dried. Dried cells were lysed in buffer A [50 mM Tris-HCl pH 7.5, 150 mM NaCl, 5 mM EDTA, 10% glycerol, 20 mM β-glycerophosphate, 0.1 mM Na_3VO_4, 10 mM p-nitrophenyl phosphate (p-NPP), 10 mM NaF] containing 0.2% NP-40 and glass beads, and disrupted by vortexing. Whole-cell extracts were mixed with 3× SDS sample buffer, and boiled for 5 min. For immunoprecipitation, exponentially grown cells were treated with 1 mM PMSF for a few minutes under shaking at 90 rpm. After centrifugation, cell pellets were washed with diluted water containing 1 mM PMSF, and frozen using liquid nitrogen. Cells were lysed in buffer B [50 mM Tris-HCl pH 7.5, 150 mM NaCl, 5 mM EDTA, 10% glycerol, 20 mM β-glycerophosphate, 0.1 mM Na_3VO_4, 10 mM p-NPP, 10 mM NaF, 1 mM PMSF, protease inhibitor cocktail and phosphatase inhibitor cocktail (Roche)] with glass beads, and then homogenized using FastPrep 24 (MP-biomedicals: 6.5 m/s, 40 s for six times with a 5 min interval on ice). Cell lysates were diluted with an equal amount of buffer B containing 0.4% NP-40 and rotated for 30 min at 4°C. After centrifugation, supernatants were incubated with anti-HA affinity matrix (Roche) or protein G–Sepharose (GE healthcare) and rabbit anti-GFP antibody (MBL; 1:400; cat. no 598) at 4°C for 4 h. Immunoprecipitants were washed three times with buffer A containing 0.1% NP-40. For Myc elution, Myc immunoprecipitants were incubated with 1 mg/ml Myc peptide solution for 15 min at 30°C two times. Cell extracts,

immunoprecipitants or Myc eluates were boiled with 3× SDS sample buffer, separated by SDS-PAGE, and then subjected to western blotting. Anti-phospho-p70 S6 K (Thr-389) antibody was purchased from Cell Signaling Technology (1:2000; cat. no 9206S). Anti-α-tubulin (B5-1-2) antibody was obtained from Sigma (1:2000; cat. no T5168). Anti-myc antibody was from Wako (1:3000; cat. no 017-21871). Anti-HA (12CA5) (1:8000; cat. no 11583816001) and mouse anti-GFP antibodies were from Roche (1:1000; cat. no 11814460001). Rabbit anti-GFP antibody was from MBL (1:1000; cat. no 598). Anti-PSTAIRE antibody was from Santa Cruz Biotechnology (1:1000; cat. no sc-53). Anti-Atg13 antibody was kindly provided by Akira Yamashita (National Institute for Basic Biology, Japan). After incubation with HRP- conjugated secondary antibodies, proteins were detected using the ECL Plus Western Blotting Substrate (Thermo Scientific). Intensities of immunoblotting bands were measured by Image J software (NIH).

RNA preparation and qPCR

Cells were cultured in EMM or EMM-NH_4Cl. RNA was extracted by disrupting cells by lysis in buffer C (0.2 M Tris-HCl pH 7.5, 0.5 M NaCl, 10 mM EDTA and 1% SDS) with glass beads. RNA was purified by removing proteins using phenol/chloroform/isoamyl alcohol mixed at 25:24:1 (pH 5.2) (Nakarai Tesque) followed by ethanol precipitation. For qPCR, 0.5 µg of total RNA was reverse transcribed to cDNA using ReverTra Ace qPCR RT Master Mix (TOYOBO). qPCR was performed using LightCycler 480 (Roche) and THUNDERBIRD SYBR qPCR Mix (TOYOBO). Primer sequences are described below. qPCR primerd were: *ste11*, forward primer 5′-CTTCTTACCCAGCAATGAGT-3′, reverse primer 5′-CAATTCTTGAGAATGAGCGG-3′; *mei2*: forward primer 5′-TGGAATTGACACAAGAACCA-3′, reverse primer 5′-GAGTACCCAC-TCTAGCTTTG-3′.

Fluorescence microscopy

To calculate mating efficiency, cells were treated with 70% ethanol, and then stained with DAPI. Non-mating cells, zygote, ascus and free-spore were distinguished, respectively, by using the fluorescence microscopy BZ-8000 (Kyence). Mating efficiency was calculated as ratio of the number of diploid cells to total cells. To visualize vacuoles, cells were incubated with FM4-64 (Invitrogen/Thermo Fisher) for 30 min at 30°C under shaking at 110 rpm. Cells were grown in filtrated EMM on a lectin-coated glass-bottomed dish (Greiner) followed by image analysis using fluorescent microscopy BZ-9000 (kyence). BZ-analyzer software (kyence) was employed for measuring the size of vacuole and fluorescence intensity.

Statistical analysis

The data are shown as the mean±s.e.m. of the indicated number of observations. To determine significant differences, Student's *t*-tests and one-way analysis of variance (ANOVA) were performed using Prism ver. 8. $P<0.05$ was considered statistically significant.

Acknowledgements

The authors thank Mrs. Shino Oguri for her administrative support and warm encouragement. The authors also appreciate Satoshi Kawamoto, Taiki Nagano, Moena Okahisa, and Yui Miyamoto for their technical support. The authors also appreciate Drs Masamitsu Sato, Fuyuhiko Tamanoi, Akira Yamashita, Masayuki Yamamoto, and the National BioResource Project (NBRP) of the MEXT, Japan for providing *S. pombe* strains, plasmids and antibody.

Competing interests

The authors declare no competing or financial interests.

Author contributions

Conceptualization: S.M., A.N.; Methodology: S.M., H.U., A.N.; Software: S.M., U.K., A.N.; Validation: S.M., U.K., H.U., A.N.; Formal analysis: S.M., H.U.; Investigation: S.M., H.U.; Resources: S.M., U.K., H.U., A.N.; Data curation: S.M., H.U.; Writing - original draft: S.M.; Writing - review & editing: U.K., A.N.; Visualization: S.M.; Supervision: U.K., A.N.; Project administration: S.M., A.N.; Funding acquisition: S.M., U.K., A.N.

Funding

This study was supported in part by the Japan Society for the Promotion of Science (JSPS) KAKENHI grant numbers 19K15751 (S.M.) and 26440053 (A.N.).

Supplementary information

Supplementary information available online at
https://jcs.biologists.org/lookup/doi/10.1242/jcs.247817.supplemental

References

Anandhakumar, J., Fauquenoy, S., Materne, P., Migeot, V. and Hermand, D. (2013). Regulation of entry into gametogenesis by Ste11: the endless game. *Biochem. Soc. Trans.* **41**, 1673-1678. doi:10.1042/BST20130225

Aono, S., Haruna, Y., Watanabe, Y. H., Mochida, S. and Takeda, K. (2019). The fission yeast Greatwall-Endosulfine pathway is required for proper quiescence/G. *Genes Cells* **24**, 172-186. doi:10.1111/gtc.12665

Astrinidis, A., Senapedis, W., Coleman, T. R. and Henske, E. P. (2003). Cell cycle-regulated phosphorylation of hamartin, the product of the tuberous sclerosis complex 1 gene, by cyclin-dependent kinase 1/cyclin B. *J. Biol. Chem.* **278**, 51372-51379. doi:10.1074/jbc.M303956200

Bähler, J., Wu, J. Q., Longtine, M. S., Shah, N. G., McKenzie, A., Steever, A. B., Wach, A., Philippsen, P. and Pringle, J. R. (1998). Heterologous modules for efficient and versatile PCR-based gene targeting in *Schizosaccharomyces pombe*. *Yeast* **14**, 943-951.doi:10.1002/(SICI)1097-0061(199807)14:10<943::AID-YEA292>3.0.CO;2-Y

Basi, G., Schmid, E. and Maundrell, K. (1993). TATA box mutations in the *Schizosaccharomyces pombe* nmt1 promoter affect transcription efficiency but not the transcription start point or thiamine repressibility. *Gene* **123**, 131-136. doi:10.1016/0378-1119(93)90552-E

Birot, A. (2016). Regulation of fission yeast cohesin by the Cyclin Dependent Kinase PeF1. *PhD thesis*, Bordeaux University. France.

Cao, L., Chen, F., Yang, X., Xu, W., Xie, J. and Yu, L. (2014). Phylogenetic analysis of CDK and cyclin proteins in premetazoan lineages. *BMC Evol. Biol.* **14**, 10. doi:10.1186/1471-2148-14-10

Chen, B. R., Li, Y., Eisenstatt, J. R. and Runge, K. W. (2013). Identification of a lifespan extending mutation in the *Schizosaccharomyces pombe* cyclin gene clg1+ by direct selection of long-lived mutants. *PLoS ONE* **8**, e69084. doi:10.1371/journal.pone.0069084

Chia, K. H., Fukuda, T., Sofyantoro, F., Matsuda, T., Amai, T. and Shiozaki, K. (2017). Ragulator and GATOR1 complexes promote fission yeast growth by attenuating TOR complex 1 through Rag GTPases. *Elife* **6**, e30880. doi:10.7554/eLife.30880.024

Chica, N., Rozalén, A. E., Pérez-Hidalgo, L., Rubio, A., Novak, B. and Moreno, S. (2016). Nutritional Control of Cell Size by the Greatwall-Endosulfine-PP2A·B55 Pathway. *Curr. Biol.* **26**, 319-330. doi:10.1016/j.cub.2015.12.035

Davey, J. (1998). Fusion of a fission yeast. *Yeast* **14**, 1529-1566. doi:10.1002/(SICI)1097-0061(199812)14:16<1529::AID-YEA357>3.0.CO;2-0

Dhavan, R. and Tsai, L. H. (2001). A decade of CDK5. *Nat. Rev. Mol. Cell Biol.* **2**, 749-759. doi:10.1038/35096019

Doi, A., Fujimoto, A., Sato, S., Uno, T., Kanda, Y., Asami, K., Tanaka, Y., Kita, A., Satoh, R. and Sugiura, R. (2015). Chemical genomics approach to identify genes associated with sensitivity to rapamycin in the fission yeast *Schizosaccharomyces pombe*. *Genes Cells* **20**, 292-309. doi:10.1111/gtc.12223

Egel, R., Nielsen, O. and Weilguny, D. (1990). Sexual differentiation in fission yeast. *Trends Genet.* **6**, 369-373. doi:10.1016/0168-9525(90)90279-F

Engebrecht, J. (2003). Cell signaling in yeast sporulation. *Biochem. Biophys. Res. Commun.* **306**, 325-328. doi:10.1016/S0006-291X(03)00983-5

Graeser, R., Gannon, J., Poon, R. Y., Dubois, T., Aitken, A. and Hunt, T. (2002). Regulation of the CDK-related protein kinase PCTAIRE-1 and its possible role in neurite outgrowth in Neuro-2A cells. *J. Cell Sci.* **115**, 3479-3490.

Higuchi, T., Watanabe, Y. and Yamamoto, M. (2002). Protein kinase A regulates sexual development and gluconeogenesis through phosphorylation of the Zn finger transcriptional activator Rst2p in fission yeast. *Mol. Cell. Biol.* **22**, 1-11. doi:10.1128/MCB.22.1.1-11.2002

Huang, J. and Manning, B. D. (2008). The TSC1-TSC2 complex: a molecular switchboard controlling cell growth. *Biochem. J.* **412**, 179-190. doi:10.1042/BJ20080281

Huang, D., Friesen, H. and Andrews, B. (2007). Pho85, a multifunctional cyclin-dependent protein kinase in budding yeast. *Mol. Microbiol.* **66**, 303-314. doi:10.1111/j.1365-2958.2007.05914.x

Kunitomo, H., Higuchi, T., Iino, Y. and Yamamoto, M. (2000). A zinc-finger protein, Rst2p, regulates transcription of the fission yeast *ste11*(+) gene, which encodes a pivotal transcription factor for sexual development. *Mol. Biol. Cell* **11**, 3205-3217. doi:10.1091/mbc.11.9.3205

Ma, N., Liu, Q., Zhang, L., Henske, E. P. and Ma, Y. (2013). TORC1 signaling is governed by two negative regulators in fission yeast. *Genetics* **195**, 457-468. doi:10.1534/genetics.113.154674

Malumbres, M. and Barbacid, M. (2005). Mammalian cyclin-dependent kinases. *Trends Biochem. Sci.* **30**, 630-641. doi:10.1016/j.tibs.2005.09.005

Marguerat, S., Schmidt, A., Codlin, S., Chen, W., Aebersold, R. and Bähler, J. (2012). Quantitative analysis of fission yeast transcriptomes and proteomes in proliferating and quiescent cells. *Cell* **151**, 671-683. doi:10.1016/j.cell.2012.09.019

Mata, J. and Bähler, J. (2006). Global roles of Ste11p, cell type, and pheromone in the control of gene expression during early sexual differentiation in fission yeast. *Proc. Natl. Acad. Sci. USA* **103**, 15517-15522. doi:10.1073/pnas.0603403103

Matsuda, S., Kominato, K., Koide-Yoshida, S., Miyamoto, K., Isshiki, K., Tsuji, A. and Yuasa, K. (2014). PCTAIRE kinase 3/cyclin-dependent kinase 18 is activated through association with cyclin A and/or phosphorylation by protein kinase A. *J. Biol. Chem.* **289**, 18387-18400. doi:10.1074/jbc.M113.542936

Matsuda, S., Kawamoto, K., Miyamoto, K., Tsuji, A. and Yuasa, K. (2017). PCTK3/CDK18 regulates cell migration and adhesion by negatively modulating FAK activity. *Sci. Rep.* **7**, 45545. doi:10.1038/srep45545

Matsumoto, S., Bandyopadhyay, A., Kwiatkowski, D. J., Maitra, U. and Matsumoto, T. (2002). Role of the Tsc1-Tsc2 complex in signaling and transport across the cell membrane in the fission yeast *Schizosaccharomyces pombe*. *Genetics* **161**, 1053-1063.

Matsuo, T., Otsubo, Y., Urano, J., Tamanoi, F. and Yamamoto, M. (2007). Loss of the TOR kinase Tor2 mimics nitrogen starvation and activates the sexual development pathway in fission yeast. *Mol. Cell. Biol.* **27**, 3154-3164. doi:10.1128/MCB.01039-06

Merlini, L., Dudin, O. and Martin, S. G. (2013). Mate and fuse: how yeast cells do it. *Open Biol* **3**, 130008. doi:10.1098/rsob.130008

Mikolcevic, P., Sigl, R., Rauch, V., Hess, M. W., Pfaller, K., Barisic, M., Pelliniemi, L. J., Boesl, M. and Geley, S. (2012). Cyclin-dependent kinase 16/PCTAIRE kinase 1 is activated by cyclin Y and is essential for spermatogenesis. *Mol. Cell. Biol.* **32**, 868-879. doi:10.1128/MCB.06261-11

Moreno, S., Klar, A. and Nurse, P. (1991). Molecular genetic analysis of fission yeast *Schizosaccharomyces pombe*. *Methods Enzymol.* **194**, 795-823. doi:10.1016/0076-6879(91)94059-L

Mukaiyama, H., Nakase, M., Nakamura, T., Kakinuma, Y. and Takegawa, K. (2010). Autophagy in the fission yeast *Schizosaccharomyces pombe*. *FEBS Lett.* **584**, 1327-1334. doi:10.1016/j.febslet.2009.12.037

Murai, T., Nakase, Y., Fukuda, K., Chikashige, Y., Tsutsumi, C., Hiraoka, Y. and Matsumoto, T. (2009). Distinctive responses to nitrogen starvation in the dominant active mutants of the fission yeast Rheb GTPase. *Genetics* **183**, 517-527. doi:10.1534/genetics.109.105379

Nakashima, A., Sato, T. and Tamanoi, F. (2010). Fission yeast TORC1 regulates phosphorylation of ribosomal S6 proteins in response to nutrients and its activity is inhibited by rapamycin. *J. Cell Sci.* **123**, 777-786. doi:10.1242/jcs.060319

Nakashima, A., Otsubo, Y., Yamashita, A., Sato, T., Yamamoto, M. and Tamanoi, F. (2012). Psk1, an AGC kinase family member in fission yeast, is directly phosphorylated and controlled by TORC1 and functions as S6 kinase. *J. Cell Sci.* **125**, 5840-5849. doi:10.1242/jcs.111146

Nakashima, A., Kamada, S., Tamanoi, F. and Kikkawa, U. (2014). Fission yeast arrestin-related trafficking adaptor, Arn1/Any1, is ubiquitinated by Pub1 E3 ligase and regulates endocytosis of Cat1 amino acid transporter. *Biol Open* **3**, 542-552. doi:10.1242/bio.20148367

Okazaki, K., Okazaki, N., Kume, K., Jinno, S., Tanaka, K. and Okayama, H. (1990). High-frequency transformation method and library transducing vectors for cloning mammalian cDNAs by trans-complementation of *Schizosaccharomyces pombe*. *Nucleic Acids Res.* **18**, 6485-6489. doi:10.1093/nar/18.22.6485

Otsubo, Y. and Yamamoto, M. (2012). Signaling pathways for fission yeast sexual differentiation at a glance. *J. Cell Sci.* **125**, 2789-2793. doi:10.1242/jcs.094771

Otsubo, Y., Yamashita, A., Ohno, H. and Yamamoto, M. (2014). S. pombe TORC1 activates the ubiquitin-proteasomal degradation of the meiotic regulator Mei2 in cooperation with Pat1 kinase. *J. Cell Sci.* **127**, 2639-2646. doi:10.1242/jcs.135517

Otsubo, Y., Nakashima, A., Yamamoto, M. and Yamashita, A. (2017). TORC1-dependent phosphorylation targets in fission yeast. *Biomolecules* **7**, 50. doi:10.3390/biom7030050

Otsubo, Y., Matsuo, T., Nishimura, A., Yamamoto, M. and Yamashita, A. (2018). tRNA production links nutrient conditions to the onset of sexual differentiation through the TORC1 pathway. *EMBO Rep.* **19**, e44867. doi:10.15252/embr.201744867

Pérez-Hidalgo, L. and Moreno, S. (2017). Coupling TOR to the cell cycle by the greatwall-endosulfine-PP2A-B55 pathway. *Biomolecules* **7**, 59. doi:10.3390/biom7030059

Qin, J., Kang, W., Leung, B. and McLeod, M. (2003). Ste11p, a high-mobility-group box DNA-binding protein, undergoes pheromone- and nutrient-regulated nuclear-cytoplasmic shuttling. *Mol. Cell. Biol.* **23**, 3253-3264. doi:10.1128/MCB.23.9.3253-3264.2003

Sabatinos, S. A. and Forsburg, S. L. (2010). Molecular genetics of *Schizosaccharomyces pombe*. *Methods Enzymol.* **470**, 759-795. doi:10.1016/S0076-6879(10)70032-X

Sajiki, K., Hatanaka, M., Nakamura, T., Takeda, K., Shimanuki, M., Yoshida, T., Hanyu, Y., Hayashi, T., Nakaseko, Y. and Yanagida, M. (2009). Genetic control of cellular quiescence in S. pombe. *J. Cell Sci.* **122**, 1418-1429. doi:10.1242/jcs.046466

Sato, M., Dhut, S. and Toda, T. (2005). New drug-resistant cassettes for gene disruption and epitope tagging in *Schizosaccharomyces pombe*. *Yeast* **22**, 583-591. doi:10.1002/yea.1233

Saxton, R. A. and Sabatini, D. M. (2017). mTOR signaling in growth, metabolism, and disease. *Cell* **169**, 361-371. doi:10.1016/j.cell.2017.03.035

Shimanuki, M., Chung, S. Y., Chikashige, Y., Kawasaki, Y., Uehara, L., Tsutsumi, C., Hatanaka, M., Hiraoka, Y., Nagao, K. and Yanagida, M. (2007). Two-step, extensive alterations in the transcriptome from G0 arrest to cell division in *Schizosaccharomyces pombe*. *Genes Cells* **12**, 677-692. doi:10.1111/j.1365-2443.2007.01079.x

Shin, C. S. and Huh, W. K. (2011). Bidirectional regulation between TORC1 and autophagy in *Saccharomyces cerevisiae*. *Autophagy* **7**, 854-862. doi:10.4161/auto.7.8.15696

Sugimoto, A., Iino, Y., Maeda, T., Watanabe, Y. and Yamamoto, M. (1991). *Schizosaccharomyces pombe ste11+* encodes a transcription factor with an HMG motif that is a critical regulator of sexual development. *Genes Dev.* **5**, 1990-1999. doi:10.1101/gad.5.11.1990

Swaffer, M. P., Jones, A. W., Flynn, H. R., Snijders, A. P. and Nurse, P. (2018). Quantitative phosphoproteomics reveals the signaling dynamics of cell-cycle kinases in the fission yeast *Schizosaccharomyces pombe*. *Cell Rep* **24**, 503-514. doi:10.1016/j.celrep.2018.06.036

Takahara, T. and Maeda, T. (2012). TORC1 of fission yeast is rapamycin-sensitive. *Genes Cells* **17**, 698-708. doi:10.1111/j.1365-2443.2012.01618.x

Tanaka, K. and Okayama, H. (2000). A pcl-like cyclin activates the Res2p-Cdc10p cell cycle "start" transcriptional factor complex in fission yeast. *Mol. Biol. Cell* **11**, 2845-2862. doi:10.1091/mbc.11.9.2845

Tournier, S., Gachet, Y. and Hyams, J. S. (1997). Identification and preliminary characterization of p31, a new PSTAIRE-related protein in fission yeast. *Yeast* **13**, 727-734. doi:10.1002/(SICI)1097-0061(19970630)13:8<727::AID-YEA134>3.0.CO;2-W

Urano, J., Comiso, M. J., Guo, L., Aspuria, P. J., Deniskin, R., Tabancay, A. P., Kato-Stankiewicz, J. and Tamanoi, F. (2005). Identification of novel single amino acid changes that result in hyperactivation of the unique GTPase, Rheb, in fission yeast. *Mol. Microbiol.* **58**, 1074-1086. doi:10.1111/j.1365-2958.2005.04877.x

Urano, J., Sato, T., Matsuo, T., Otsubo, Y., Yamamoto, M. and Tamanoi, F. (2007). Point mutations in TOR confer Rheb-independent growth in fission yeast and nutrient-independent mammalian TOR signaling in mammalian cells. *Proc. Natl. Acad. Sci. USA* **104**, 3514-3519. doi:10.1073/pnas.0608510104

Uritani, M., Hidaka, H., Hotta, Y., Ueno, M., Ushimaru, T. and Toda, T. (2006). Fission yeast Tor2 links nitrogen signals to cell proliferation and acts downstream of the Rheb GTPase. *Genes Cells* **11**, 1367-1379. doi:10.1111/j.1365-2443.2006.01025.x

Valbuena, N. and Moreno, S. (2010). TOR and PKA pathways synergize at the level of the Ste11 transcription factor to prevent mating and meiosis in fission yeast. *PLoS ONE* **5**, e11514. doi:10.1371/journal.pone.0011514

Valbuena, N., Guan, K. L. and Moreno, S. (2012). The Vam6 and Gtr1-Gtr2 pathway activates TORC1 in response to amino acids in fission yeast. *J. Cell Sci.* **125**, 1920-1928. doi:10.1242/jcs.094219

van Slegtenhorst, M., Carr, E., Stoyanova, R., Kruger, W. D. and Henske, E. P. (2004). $Tsc1^+$ and $tsc2^+$ regulate arginine uptake and metabolism in *Schizosaccharomyces pombe*. *J. Biol. Chem.* **279**, 12706-12713. doi:10.1074/jbc.M313874200

van Slegtenhorst, M., Mustafa, A. and Henske, E. P. (2005). Pas1, a G1 cyclin, regulates amino acid uptake and rescues a delay in G1 arrest in Tsc1 and Tsc2 mutants in *Schizosaccharomyces pombe*. *Hum. Mol. Genet.* **14**, 2851-2858. doi:10.1093/hmg/ddi317

Yang, Z., Geng, J., Yen, W. L., Wang, K. and Klionsky, D. J. (2010). Positive or negative roles of different cyclin-dependent kinase Pho85-cyclin complexes orchestrate induction of autophagy in *Saccharomyces cerevisiae*. *Mol. Cell* **38**, 250-264. doi:10.1016/j.molcel.2010.02.033

Yu, L., McPhee, C. K., Zheng, L., Mardones, G. A., Rong, Y., Peng, J., Mi, N., Zhao, Y., Liu, Z., Wan, F. et al. (2010). Termination of autophagy and reformation of lysosomes regulated by mTOR. *Nature* **465**, 942-946. doi:10.1038/nature09076